Theories for design and analysis of robust H ∞ / H – fault detectors

David Henry

Theories for design and analysis of robust H_∞/H_- fault detectors

David Henry[a]

[a]*IMS lab., Univ. Bordeaux, Bordeaux INP, CNRS (UMR 5218), 351 Cours de la libération, 33405, Talence, France*

Abstract

This paper deals with model-based fault detection and isolation problems, for linear time invariant systems subject to a large class of uncertainties and disturbances. A new approach based on non-smooth optimization techniques, is proposed to synthesize a state–space realization of the fault detection filter, within the H_∞/H_- setting. A set of new criteria for robust fault detection performance analysis is too proposed, using the generalized structured singular value theory. The proposed theories are illustrated on a satellite example, under a large class of nonlinear dependent uncertainties. Through a deep analysis of the example, it is shown how the H_∞/H_- design – μ_g analysis tools can serve as a general theory, to solve fault detection problems.

Keywords: Robust fault detection and isolation, H_∞/H_- filters, generalized structured singular value μ_g.

1. Introduction

Design and analysis of model–based Fault Detection and Isolation (FDI) solutions, becomes more and more of interest in practical applications. Intensive attention has been drawn during last decades, on the design of FDI schemes, see the surveys [12, 53]. The proposed techniques can be brought down to two concepts: Fault estimation and residual generation.

Residual generation is different from fault estimation because it does only require disturbances and model perturbations attenuation. The residuals have to remain sensitive to faults while guaranteeing robustness against model perturbations and unknown inputs. This means that, as opposed to a fault estimation problem which is fundamentally a minimisation problem (we look for the fault estimate to be minimal, in some criteria sense), a residual generation problem is a minimisation/maximisation problem.

One historically distinguishes three main categories of residual generation techniques, the parity space technique, see the recent developments reported in [38, 50, 48], the observer–based approach and the so-called direct filtering approaches.

The observer–based approach is probably the most studied technique. One of the most successful robust observer techniques for fault diagnosis is the Unknown Input Observer (UIO) technique,

Email address: david.henry@ims-bordeaux.fr (David Henry)

see [30, 17, 40] to name a few recent results. Unfortunately, these observers are designed under pure robustness constraints, and fault sensitivity performances are mainly checked *a posteriori*. In many cases, this results in a rank condition. The mixed H_∞/H_- observer technique aims at proposing a solution to this problem. The authors of the papers [24, 25, 46] were the precursors to propose a well posed definition of the H_- criteria for fault sensitivity measure, in the sense that it does not require the full-rank column condition of the D-matrix. It seems now that this latest definition is well admitted [44, 45, 47, 52], thanks to the generalized Kalman–Yakubovich–Popov lemma [27] that gives an exact linear matrix inequality (LMI) characterization of the H_- index in a finite frequency domain.

The direct filtering approach looks for a state–space realization. In this sense, this approach presents more degrees of freedom than an observer–based solution, since, first, the structure of the residual generator is not *a priori* fixed, and, second, it can be of higher order than an observer, which is a clear advantage from a performance point of vue. The theoretical foundations of the direct filtering approach come mainly from the H_∞/μ robust control community. That is why pure H_∞ solutions, as well as μ-synthesis solutions, have been proposed in the past, see [42, 41, 26, 31] to name a few papers. With the aid of the recent developments in the H_∞/μ robust control theory, recent theories address mixed criteria such as H_∞/H_∞ [11], H_2/H_∞ [29], H_∞/H_- [11, 24, 26, 21, 23] and $H_\infty/H_-/H_{2g}$ with LMI regions constraints [34, 25].

The fault detector design problem addressed in this paper, obeys to the direct filtering approach. More precisely, the theoretical developments are proposed within the H_∞/H_- setting that uses the LFT paradigm. The contributions of the paper are twofold:

i) The paper proposes a new H_∞/H_- design theory that looks for a state–space realization of the fault detection filter, under fixed structure and/or tunable parameters. The problem is formulated as a non-smooth optimization problem. This is the first contribution of the paper.

ii) Following the μ-analysis philosophy of the H_∞ robust control community, a set of new indicators for robust fault detection performance analysis is proposed within the H_∞/H_- framework. These indicators are developed within the generalized structured singular value μ_g framework. The aim is to provide μ_g tools for worst-case performance analysis and margins of H_∞/H_- robust fault detectors. These new tools are the second contribution of the paper.

The proposed theories are illustrated on a satellite's example, that considers flexible modes of the solar arrays and a large class of nonlinear dependent uncertainties, i.e. satellite and solar array inertias, and frequencies and damping factors of the flexible modes. Through a deep analysis of the example, it is shown how the H_∞/H_- design – μ_g analysis tools can serve as a general theory, to assess and enhance the robust performances of any kind of LTI fault detection filter, in a very efficient way.

The paper is organized as follows. Section 2 states the problem. Section 3 is dedicated to the H_∞/H_- design theories. A slightly extended version of the full order design procedure proposed in [24] is first establsihed in terms of a LMI optimization problem. Then, a new approach based on non-smooth optimization techniques, is proposed. Section 4 is dedicated to the μ_g tools. The μ_g analysis procedure proposed in [24] is briefly recalled as a necessary background for the new μ_g–based analysis tools. Finally, section 5 is devoted to the satellite example.

Notations

The notations are those used in the majority of H_∞/μ literature. $\overline{\sigma}(A)/\underline{\sigma}(A)$ denote the maximum/minimum singular values of the matrix A. $\|w\|_2$ is used to denote the L_2-norm of the signal w. A transfer $P(s)$ where "s" is the Laplace variable, denoted simply P, is assumed to be in $\mathbb{R}H_\infty$, real rational function with $||P||_\infty = \sup_\omega \overline{\sigma}(P(j\omega)) < \infty$ ($||P||_\infty$ is also the largest gain of P). For LTI systems, $||P||_\infty$ is accompanied by the non-zero smallest gain of P, that is the H_- index given in a finite frequency range, which is the restriction of $\inf_\omega \underline{\sigma}(P(j\omega))$ to a finite frequency domain Ω, i.e., $||P||_- = \inf_{\omega\in\Omega} \underline{\sigma}(P(j\omega)) \neq 0$. The notation $P = \left[\begin{array}{c|c} A & B \\ \hline C & D \end{array}\right]$ is used to refer to the state-space model $P : \left\{ \begin{array}{l} \dot{x} = Ax + Bu \\ y = Cx + Du \end{array} \right.$. Linear Fractional Transformations (LFTs) are extensively used in the paper. For appropriately dimensioned matrices N and $M = \left(\begin{array}{cc} M_{11} & M_{12} \\ M_{21} & M_{22} \end{array} \right)$, the lower LFT is defined according to $\mathcal{F}_l(M,N) = M_{11} + M_{12}N(I - M_{22}N)^{-1}M_{21}$ and the upper LFT as $\mathcal{F}_u(M,N) = M_{22} + M_{21}N(I - M_{11}N)^{-1}M_{12}$, under the assumption that the involved matrix inverses exist. This assumption is discussed in the paper when it is judged necessary. Otherwise, it is assumed to be satisfied. $M \star N$ refers to the Redheffer star product which is defined by $M \star N = \begin{bmatrix} \mathcal{F}_l(M, N_{11}) & M_{12}(I - N_{11}M_{22})^{-1}N_{12} \\ N_{21}(I - M_{22}N_{11})^{-1}M_{21} & \mathcal{F}_u(N, M_{22}) \end{bmatrix}$. Consider a block structure $\underline{\Delta} = \text{diag}(\underline{\Delta}_J, \underline{\Delta}_K)$ so that $\underline{\Delta}_J = \Big\{\text{bloc diag}(\delta_1^r I_{k_1}, ..., \delta_{m_{rJ}}^r I_{k_{m_{rJ}}}, \delta_1^c I_{k_{m_{rJ}+1}}, ..., \delta_{m_{cJ}}^c I_{k_{m_{rJ}+m_{cJ}}}, \Delta_{J1}^C, ..., \Delta_{Jm_{CJ}}^C)\Big\}$ and $\underline{\Delta_K} = \big\{\text{bloc diag}(\Delta_{K1}^C, ..., \Delta_{Km_{CK}}^C)\big\}$ with $\delta^r \in \mathbb{R}, \delta^c \in \mathbb{C}, \Delta^C \in \mathbb{C}$ and consider a complex valued matrix $M = \left(\begin{array}{cc} M_{JJ} & M_{JK} \\ M_{KJ} & M_{KK} \end{array} \right)$ partitioned in accordance with $\underline{\Delta}$, which define the closed-loop equations $z = Mv, \quad v = \Delta z, \quad z = (z_j^T \ z_k^T)^T$, $v = (v_j^T \ v_k^T)^T$ where Δ_J and Δ_K satisfy respectively a maximum norm constraint and a minimum gain constraint. Then, the μ_g-function is a positive real-valued function of the matrix M and the specified perturbation block $\underline{\Delta}$ defined by $\mu_{g\underline{\Delta}}(M) \stackrel{\Delta}{=} \max_{\|v\|=1} \left\{ \gamma : \begin{array}{l} \|v_j\|\gamma \leq \|z_j\|, \forall j \in J \\ \|v_k\| \geq \|z_k\|\gamma, \forall k \in K \end{array} \right\}$ and is defined on a domain $\text{dom}(\mu_g)$ given by $M \in \text{dom}(\mu_g)$ iff $M_{KK}v_K = 0 \Rightarrow v_K = 0$.

2. Problem statement

Consider the fault detection design problem given by Fig. 1.a. The system model consists of a nominal LTI model G and a perturbation bloc $\Delta \in \mathbb{B}_\Delta$ with $\mathbb{B}_\Delta = \{\Delta \in \underline{\Delta} : \overline{\sigma}(\Delta) \leq 1\}$, acting on the nominal model, such that

$$\underline{\Delta} = \big\{\text{block diag}(\delta_1^r I_{k_1}, ..., \delta_{m_r}^r I_{k_{m_r}}, \delta_1^c I_{k_{m_r+1}}, ..., \delta_{m_c}^c I_{k_{m_r+m_c}}, \Delta_1^C, ..., \Delta_{m_C}^C)\big\} \tag{1}$$

where $\delta^r \in \mathbb{R}, \delta^c \in \mathbb{C}, \Delta^C \in \mathbb{C}$ are referred as repeated real, repeated complex and complex linear time-invariant dynamic uncertainties [13, 51]. It is assumed that all model perturbations (e.g. parametric uncertainties and neglected dynamics) are represented by Δ. $d \in \mathbb{R}^{q_d}$ and $f \in \mathbb{R}^{q_f}$ also refer to disturbances and faults to be detected, respectively. K is a LTI controller, that is assumed to be known. $\eta \in \mathbb{R}^{q_\eta}$ and $\zeta \in \mathbb{R}^{q_\zeta}$ are internal signals.

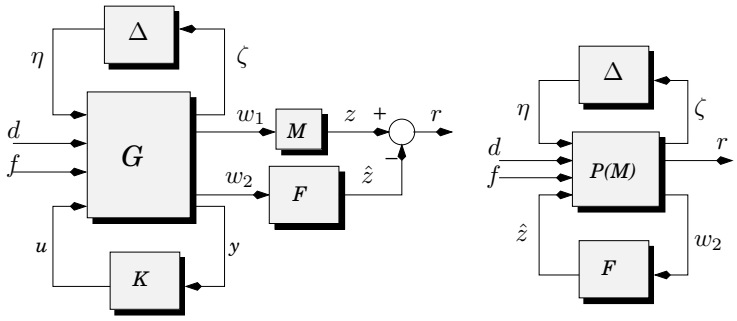

Figure 1: a): The H_∞/H_- synthesis problem (left) and b): its equivalent form (right).

The problem to be solved is formulated as follows: we look for a linear combination $z \in \mathbb{R}^q$ of some system's outputs $w_1 \in \mathbb{R}^{m_1}$, that is $z = Mw_1$, and its estimate $\hat{z}$, by filtering through a dynamic filter F, some system's outputs $w_2 \in \mathbb{R}^{m_2}$ that are not necessarily the same, i.e. w_1 and w_2 may differ. Then, $r = z - \hat{z}$ defines a residual vector, since it will be close to zero if $\hat{z}$ tends to z when $f = 0$ and whenever the presence of disturbances d and model perturbations Δ. However, when $f \neq 0$, z must differ as much as possible from its estimate $\hat{z}$, if we want r to be a good residual vector. The variables to be designed are then the state–space matrices $A_F \in \mathbb{R}^{n_F \times n_F}$, $B_F \in \mathbb{R}^{n_F \times m_2}$, $C_F \in \mathbb{R}^{q \times n_F}, D_F \in \mathbb{R}^{q \times m_2}$ of $F = \left[\begin{array}{c|c} A_F & B_F \\ \hline C_F & D_F \end{array}\right]$ and the matrix $M \in \mathbb{R}^{q \times m_1}$.

The following assumption about fault detectability, is made.

Assumption 1. *[39] There exist a positive scalar ν and a residual generator $r = \Psi(d, f)$ such that, for all $\rho > 0$ and all $\Delta \in \mathbb{B}_\Delta$, $||\Psi(d,0)||_2 \leq \rho||d||_2$ $\forall d$ and $||\Psi(d,f)||_2 \geq \nu||f||_2$ $\forall d$ and $\forall f$.*

Using LFT algebra manipulations, it can be verified that the diagram illustrated on Fig.1.a admits the following expression, given in the Laplace domain, see Fig.1.b:

$$r(s) = T_{vr}(\Delta, M, s)v(s) \quad T_{vr}(\Delta, M) = \mathcal{F}_l\left(\mathcal{F}_u\left(P(M), \Delta\right), F\right) \quad v = \left[d^T \; f^T\right]^T \tag{2}$$

In this equation, $T_{vr}(\Delta, M)$ denotes transfer associated to the channel $v = \left[d^T \; f^T\right]^T \rightarrow r$, that depends on the model perturbations Δ.

With $r, z, \hat{z}$ defined as previously, the goal turns out to be the design of the (stable) filter realization matrices A_F, B_F, C_F, D_F and the matrix M that solve the following H_∞/H_- optimization problem

$$\min_{M,F} \gamma_1 \quad \begin{array}{l} \forall \Delta \in \mathbb{B}_\Delta \\ \text{s.t.} ||T_{dr}(\Delta, M)||_\infty < \gamma_1 \end{array} \tag{3}$$

$$\max_{M,F} \gamma_2 \quad \begin{array}{l} \forall \omega \in \Omega, \quad \forall \Delta \in \mathbb{B}_\Delta \\ \text{s.t.} ||T_{fr}(\Delta, M)||_- > \gamma_2 \end{array} \tag{4}$$

where $T_{dr}(\Delta, M)$ and $T_{fr}(\Delta, M)$ are deduced from $T_{vr}(\Delta, M)$ given by Eq. (2), by selecting

the adequate channels. $T_{dr}(\Delta, M)$ is then the (closed-loop) transfer associated to the channel $d \to r$, and $T_{fr}(\Delta, M)$ refers to the (closed-loop) transfer associated to the channel $f \to r$. γ_1 and γ_2 are positive scalars introduced to manage the robustness and the fault sensitivity constraints, respectively. Ω denotes the frequency range where it is required to enforce fault sensitivity.

Remark 1. *Note that the above problem formulation is a slightly extended version of the approach presented in [24], since the problem considered in [24] corresponds to the particular case* $w_1 = w_2 = \begin{bmatrix} y^T & u^T \end{bmatrix}^T$ *and* $M = \begin{bmatrix} M_y & M_u \end{bmatrix}$.

Remark 2. *In the proposed formulation, the fault detection problem is formulated considering a controller* K*, which is thought an advantage since it is well known that the control actions can cover the fault effects. This benefit has been already discussed in [24]. However, an open-loop formulation may be required for some particular systems. For such cases, the fault detection problem can be easily derived from the aforementioned problem formulation, by simply removing* K*. It follows that the vector* v *entering in Eq. 2, will be augmented by the command input vector* u*. However, it should be outlined that, i) the system under consideration has to be stable which is not a strong limitation since an unstable system rarely operates in open loop, and ii) the signals* w_1, w_2 *must contain* u*, to enforce* u *to enter* F*. Towards this end, we argue that the theories developed in this paper, can be used without loss of generality.*

3. The H_∞/H_- design theory

3.1. LMI solution

In the interest of brevity, throughout this section an earnest attempt will be made to avoid duplicating material presented in [24]. Towards this end, the focus of this section will lie wholly with the results summarized by theorem 1.

Following the method proposed in [24], the robustness and fault sensitivity requirements (3) and (4) are expressed in terms of desired gain responses for the transfers $T_{dr}(\Delta, M)$ and $T_{fr}(\Delta, M)$. This is done through dynamical weights W_d and W_f, respectively. Then, a key ingredient in the theory presented in [24], is lemma 2 that states that a sufficient condition for requirements (3) and (4) to be satisfied is

$$||T_{dr}(\Delta, M)W_d^{-1}||_\infty < 1 \text{ and } ||T_{f\tilde{r}}(\Delta, M)||_\infty < 1 \tag{5}$$

where W_d and W_f have been scaled such that $||W_d||_\infty \leq \gamma_1$ and $||W_f||_- \geq \gamma_2$. $\tilde{r}$ is a fictitious signal defined such that $\tilde{r} = r - W_F f$ with $||W_F||_- = \frac{1+\gamma_2}{\gamma_2}||W_f||_-$. $T_{f\tilde{r}}(\Delta, M)$ also denotes the transfer associated to the channel $f \to \tilde{r}$.

Based on this property, the H_∞/H_- filter design problem can be re-casted in a fictitious H_∞-framework so that

$$\begin{bmatrix} r(s) \\ \tilde{r}(s) \end{bmatrix} = \mathcal{F}_l\left(\mathcal{F}_u\left(\tilde{P}(M,s), \Delta(s)\right), F(s)\right)\begin{bmatrix} \tilde{d}(s) \\ f(s) \end{bmatrix} \tag{6}$$

in which $\tilde{d}$ is the fictitious signal generating d through W_d^{-1}, see Fig. 2 that helps to follow the LFT manipulations. Then, by virtue of the small gain theorem, a sufficient condition for (5) to hold is

$$\left\|\mathcal{F}_l\left(\tilde{P}(M), F\right)\right\|_\infty < 1 \tag{7}$$

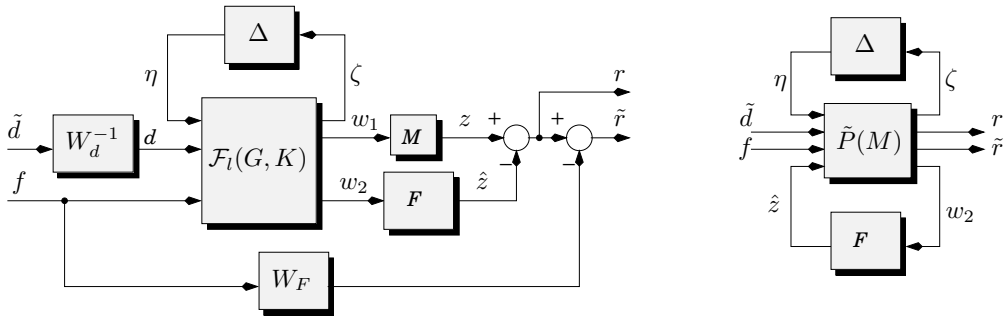

Figure 2: a:) The weighted H_∞/H_- synthesis problem (left) and b): its standard form (right).

Let us denote the state–space realizations of W_d^{-1}, W_F and $\mathcal{F}_l(G,K)$ as follows

$$W_d^{-1} = \left[\begin{array}{c|c} A_{wd} & B_{wd} \\ \hline C_{wd} & D_{wd} \end{array}\right] \quad W_F = \left[\begin{array}{c|c} A_{wF} & B_{wF} \\ \hline C_{wF} & D_{wF} \end{array}\right] \quad \mathcal{F}_l(G,K) = \left[\begin{array}{c|ccc} A & B_\eta & B_d & B_f \\ \hline C_\zeta & D_{\zeta\eta} & D_{\zeta d} & D_{\zeta f} \\ C_1 & D_{1\eta} & D_{1d} & D_{1f} \\ C_2 & D_{2\eta} & D_{2d} & D_{2f} \end{array}\right] \tag{8}$$

Then, it can be verified that the state–space realization of $\tilde{P}(M)$ is given by

$$\tilde{P}(M) = \left[\begin{array}{c|cc} \tilde{A} & \tilde{B}_1 & \tilde{B}_2 \\ \hline \tilde{C}_1 & \tilde{D}_{11} & \tilde{D}_{12} \\ \tilde{C}_2 & \tilde{D}_{21} & \tilde{D}_{22} \end{array}\right] = \left[\begin{array}{ccc|ccc:c} A & B_dC_{wd} & 0 & B_\eta & B_dD_{wd} & B_f & 0 \\ 0 & A_{wd} & 0 & 0 & B_{wd} & 0 & 0 \\ 0 & 0 & A_{wF} & 0 & 0 & B_{wF} & 0 \\ \hline C_\zeta & D_{\zeta d}C_{wd} & 0 & D_{\zeta\eta} & D_{\zeta d}D_{wd} & D_{\zeta f} & 0 \\ MC_1 & 0 & 0 & MD_{1\eta} & MD_{1d} & MD_{1f} & -I_q \\ MC_1 & 0 & -C_{wF} & MD_{1\eta} & MD_{1d} & MD_{1f} - D_F & -I_q \\ \hdashline C_2 & 0 & 0 & D_{2\eta} & D_{2d} & D_{2f} & 0 \end{array}\right] \tag{9}$$

with $\tilde{A} \in \mathbb{R}^{n\times n}$, $\tilde{B}_1 \in \mathbb{R}^{n\times(q_\eta+q_d+q_f)}$, $\tilde{B}_2 \in \mathbb{R}^{n\times q}$, $\tilde{C}_1 \in \mathbb{R}^{(q_\zeta+2q)\times n}$ and $\tilde{C}_2 \in \mathbb{R}^{m_2\times n}$. The dimensions of $\tilde{D}_{11}, \tilde{D}_{12}, \tilde{D}_{21}$ and $\tilde{D}_{22}$ can be easily determined from those dimensions.

The following theorem solves the problem.

Theorem 1. *Let $\mathcal{W} = \begin{bmatrix}\tilde{C}_2 & \tilde{D}_{21}\end{bmatrix}^\perp$. Then there exist M, A_F, B_F, C_F and D_F such that Eq. (7) is satisfied if and only if there exist M, two symmetric matrices $R, S \in \mathbb{R}^{n\times n}$ and a scalar $\gamma < 1$ such that the following system of LMIs is feasible:*

$$\begin{bmatrix} \tilde{A}R + R\tilde{A}^T & R\begin{bmatrix}C_\zeta & D_{\zeta d}C_{wd} & 0\end{bmatrix}^T & \tilde{B}_1 \\ \begin{bmatrix}C_\zeta & D_{\zeta d}C_{wd} & 0\end{bmatrix}R & -\gamma I & \begin{bmatrix}D_{\zeta\eta} & D_{\zeta d}D_{wd} & D_{\zeta f}\end{bmatrix} \\ \tilde{B}_1^T & \begin{bmatrix}D_{\zeta\eta} & D_{\zeta d}D_{wd} & D_{\zeta f}\end{bmatrix}^T & -\gamma I \end{bmatrix} < 0 \tag{10}$$

$$\begin{bmatrix} \mathcal{W} & 0 \\ 0 & I \end{bmatrix}^T \begin{bmatrix} \tilde{A}^TS + S\tilde{A} & S\tilde{B}_1 & \tilde{C}_1^T(M) \\ \tilde{B}_1^TS & -\gamma I & \tilde{D}_{11}^T(M) \\ \tilde{C}_1(M) & \tilde{D}_{11}(M) & -\gamma I \end{bmatrix} \begin{bmatrix} \mathcal{W} & 0 \\ 0 & I \end{bmatrix} < 0 \tag{11}$$

$$\begin{bmatrix} R & I \\ I & S \end{bmatrix} > 0 \tag{12}$$

Then, $n_F = n$, i.e. F is a full order solution. Moreover, F is of order $n_r < n_F$ if for some M, R, S, γ, $rank(I - RS) \leq n_r$.

Proof: Direct application of proposition 4 in [24] to $\tilde{P}(M)$ given by Eq. (9). □

The matrices A_F, B_F, C_F and D_F of the fault detection filter can then be computed from any solution M, R, S, γ. In particular, one can look for the minimal value of γ by solving the optimisation problem "$\min \gamma$ s.t. Eq. (10)-(12)". Then, the approach proposed in [16] can be used to derive A_F, B_F, C_F and D_F from the optimal solution M^*, R^*, S^*, γ^*.

3.2. Non smooth formulation

Let us now consider the following restrictions on Δ.

Assumption 2. *The uncertainty block Δ given by Eq. (1) has no complex terms δ^c i.e. $\Delta =$ block diag$(\delta_1^r I_{k_1}, ..., \delta_{m_r}^r I_{k_{m_r}}, \Delta_1^C, ..., \Delta_{m_C}^C)$. Furthermore, the elements of the full complex block Δ^C are assumed to be square $\Leftrightarrow q_{\eta_i} = q_{\zeta_i}, i = 1, ..., m_C$.*

Assumption 2 is thought without loss of generality since Δ covers both real uncertainties and complex LTI dynamic uncertainties, and then covers all practical cases. Furthermore, it is always possible to square down the model $\tilde{P}$ in (9) with respect to $\{$block diag$(\Delta_i^C)\}, i = 1, ..., m_C$.

With the help of Fig. 2.b, it can be seen that, by definition (from now on the dependence of M is omitted for clarity):

$$\mathcal{F}_l\left(\mathcal{F}_u\left(\tilde{P}, \Delta\right), F\right) = \begin{bmatrix} T_{\tilde{d}r}(\Delta) & T_{fr}(\Delta) \\ T_{\tilde{d}\tilde{r}}(\Delta) & T_{f\tilde{r}}(\Delta) \end{bmatrix} \tag{13}$$

where $T_{io}(\Delta) : o(s) = T_{io}(\Delta, s)i(s)$ denotes the transfer from the input "i" to the output "o". It follows that the solution derived from theorem 1 may be conservative, since:

- first, it is based on the small gain theorem to remove Δ from the problem, i.e. Eq. (7) is a sufficient condition for $\left\|\mathcal{F}_l\left(\mathcal{F}_u\left(\tilde{P}, \Delta\right), F\right)\right\|_\infty < 1, \forall \Delta \in \mathbb{B}_\Delta$. In other words, the LMIs (10)-(12) do neither consider the block-diagonal structure of Δ nor its nature (real,complex or mixed real-complex).
- second, it implicitly considers the off-diagonal terms $T_{fr}(\Delta)$ and $T_{\tilde{d}\tilde{r}}(\Delta)$ of Eq. (13).

The second problem can be managed adequately, by introducing judiciously chosen weighting functions on $T_{fr}(\Delta)$ and $T_{\tilde{d}\tilde{r}}(\Delta)$ as it has been done in e.g. [24, 25, 26, 19, 21]. However, the first problem remains. This is the price to pay to have a convex formulation in terms of LMIs.

To overcome these problems, it is proposed in the following, to use the nonsmooth theory proposed in [10]. This technique enables to consider the nature of Δ and its block-diagonal structure under assumption 2, and to vanish the influence of the off-diagonal terms $T_{fr}(\Delta)$ and $T_{\tilde{d}\tilde{r}}(\Delta)$ occurring in the transfer described by Eq. (13). This is in fact, the problem as it is stated in section 3.1. Another benefit is the possibility to structure the filter F, i.e. we can choose for F, a fixed

structure and/or a fixed order and/or fixed parameters.

To proceed, let us first outline that the transfer $T_{dr}(\Delta)W_d^{-1}$ that appears in the developments presented in section 3.1, is nothing else than the top left transfer $T_{\tilde{d}r}(\Delta)$ in Eq. (13). Then, the requirement $||T_{dr}(\Delta)W_d^{-1}||_\infty = ||T_{\tilde{d}r}(\Delta)||_\infty < 1$ can be rewritten according to

$$\left\|\mathcal{F}_l\left(\mathcal{F}_u\left(\tilde{P}_1,\Delta\right),F\right)\right\|_\infty < 1 \text{ with } \tilde{P}_1 = \left[\begin{array}{cc|ccc} A & B_dC_{wd} & B_\eta & B_dD_{wd} & 0 \\ 0 & A_{wd} & 0 & B_{wd} & 0 \\ \hline C_\zeta & D_{\zeta d}C_{wd} & D_{\zeta\eta} & D_{\zeta d}D_{wd} & 0 \\ MC_1 & 0 & MD_{1\eta} & MD_{1d} & -I_q \\ C_2 & 0 & D_{2\eta} & D_{2d} & 0 \end{array}\right] \tag{14}$$

Similarly, noticing that the transfer $T_{f\tilde{r}}(\Delta)$ is located at the bottom right position in Eq. (13), it follows that the requirement $||T_{f\tilde{r}}(\Delta)|| < 1$ can be rewritten according to

$$\left\|\mathcal{F}_l\left(\mathcal{F}_u\left(\tilde{P}_2,\Delta\right),F\right)\right\|_\infty < 1 \text{ with } \tilde{P}_2 = \left[\begin{array}{cc|ccc} A & 0 & B_\eta & B_f & 0 \\ 0 & A_{wF} & 0 & B_{wF} & 0 \\ \hline C_\zeta & 0 & D_{\zeta\eta} & D_{\zeta f} & 0 \\ MC_1 & -C_{wF} & MD_{1\eta} & MD_{1f}-D_F & -I_q \\ C_2 & 0 & D_{2\eta} & D_{2f} & 0 \end{array}\right] \tag{15}$$

So the goal we pursue is to derive M and a (stable) filter F so that (14) and (15) are satisfied, with some *a priori* chosen constraints on F. Especially, we would like to consider for F, some *a priori* fixed structure and/or tunable parameters.

To proceed, $\mathcal{F}_l\left(\mathcal{F}_u\left(\tilde{P}_1,\Delta\right),F\right)$ and $\mathcal{F}_l\left(\mathcal{F}_u\left(\tilde{P}_2,\Delta\right),F\right)$ are merged into a unique LFT, which leads to a new LFT $\mathcal{F}_l\left(\mathcal{F}_u\left(\hat{P},\hat{\Delta}\right),diag(F,F)\right)$, where $\hat{\Delta} = \text{diag}(\delta_1^r I_{2.k_1},...,\delta_{m_r}^r I_{2.k_{m_r}},\Delta_1^C I_2,...,\Delta_{m_C}^C I_2)$ is deduced from $diag(\Delta,\Delta)$ by reorganising its elements. Then the problem turns out to be the design of (F,M), such that:

$$\left\|\mathcal{F}_l\left(\mathcal{F}_u\left(\hat{P},\hat{\Delta}\right),\hat{F}\right)\right\|_\infty < 1 \tag{16}$$

s.t. $\hat{F} = diag(F,F)$, F is stable $\forall\hat{\Delta} : \overline{\sigma}(\hat{\Delta}) \leq 1$, and F has fixed structure and/or tunable parameters

The solution to this problem is given by the following theorem, whose foundations are mainly inspired by the $D-G$ scaling matrices technique, of the μ theory [13, 51]:

Theorem 2. *Consider assumption 2. With the real uncertain blocks $\delta_i^r I_{2.k_i}$ entering in $\hat{\Delta}$, let us associate stable dynamic multipliers $\mathcal{M} \in \underline{\mathcal{M}}$ where $\underline{\mathcal{M}} := \{\mathcal{M}(s) = \text{diag}(\mathcal{M}_i(s)) : ||\mathcal{M}_i||_\infty < 1\}$ where $\mathcal{M}(s)$ commutes with $\text{diag}(\delta_i^r I_{2.k_i})$, $i = 1,...,m_r$. With the complex block Δ^C entering in $\hat{\Delta}$, let us associate the set $\underline{\mathcal{D}}$ of D-scalings so that $\underline{\mathcal{D}} := \left\{\mathcal{D}(s) = \text{diag}(\mathcal{D}_i(s)I_{k_i}) : \mathcal{D}_i(s), \mathcal{D}_i^{-1}(s) \text{ stable }\right\}$ that commutes with $\text{diag}(\Delta_i^C), i = 1,...,2.m_C$. If there exist $\mathcal{M} \in \underline{\mathcal{M}}$, $\mathcal{D} \in \underline{\mathcal{D}}$, (M,F), $0 < \gamma < 1$*

and a small $\alpha > 0$ *that solve*

$$\begin{aligned} &\min \gamma \\ &s.t. \left\| \mathcal{F}_l\left(\mathcal{F}_u\left(\hat{P}_\gamma, \Gamma(\mathcal{M},\mathcal{D})\right), \hat{F}\right)\right\|_\infty \leq 1-\alpha \\ &\quad \mathcal{F}_l\left(\mathcal{F}_u\left(\hat{P}_\gamma, \Gamma(\mathcal{M},\mathcal{D})\right), \hat{F}\right) \text{internally stable} \\ &\quad ||\mathcal{M}||_\infty \leq 1-\alpha \\ &\quad F \text{ has fixed structure and/or tunable parameters} \end{aligned} \tag{17}$$

then (M, F) *solves* (16). *In* (17), $\Gamma(\mathcal{M},\mathcal{D}) = \begin{bmatrix} \mathcal{M} & 0 & I-\mathcal{M} & 0 \\ 0 & 0 & 0 & \mathcal{D}^{-1} \\ I+\mathcal{M} & 0 & -\mathcal{M} & 0 \\ 0 & \mathcal{D} & 0 & 0 \end{bmatrix}$ *and* $\hat{P}_\gamma$ *corresponds to* $\hat{P}$ *whose channel* $[\tilde{d}^T \ f^T]^T \to [r^T \ \tilde{r}^T]^T$ *has been scaled by* $1/\gamma$.

Proof: Direct application of theorem 1 and corollary 1 in [10], to $\mathcal{F}_l\left(\mathcal{F}_u\left(\hat{P}, \hat{\Delta}\right), \hat{F}\right)$. □

In this theorem, the free parameters are the components of the matrices M, A_F, B_F, C_F, D_F, and the components of the state space matrices associated to $\mathcal{M}(s), \mathcal{D}(s)$. Let us gather them into a vector $\mathbf{x} \in \mathbb{R}^{q_\mathbf{x}}$. Then, if we omit the constraint about the structure of F and the tunable parameters, the optimization problem (17) can be rewritten according to the following program

$$\min_{\mathbf{x}\in\mathbb{R}^{q_\mathbf{x}}} f_\infty(\mathbf{x}) \triangleq \max_{\omega\in[0,+\infty]} f(\omega, \mathbf{x}) \tag{18}$$

This optimisation problem is the composition of the H_∞ norm, which is convex but a nonsmooth function, with the LFTs $\mathbf{x} \to \mathcal{F}_l(\bullet(j\omega), \mathbf{x})$ and $\mathbf{x} \to \mathcal{F}_u(\bullet(j\omega), \mathbf{x})$, which define a non-convex but differentiable mapping. Such a problem can be solved using the technique proposed in [2]. The key property is that the functions $\mathcal{F}_l(\bullet(j\omega), \mathbf{x})$ and $\mathcal{F}_u(\bullet(j\omega), \mathbf{x})$ are Clarke regular which means that a complete description of the Clarke subdifferential $\partial f(\mathbf{x})$ can be calculated [7]. This property allows to distinguish between critical points including local minima $\mathbf{x}$, that is points $\mathbf{x}$ so that $0 \in \partial f(\mathbf{x})$, from points $\mathbf{x}$ that must be discarded, i.e. $0 \notin \partial f(\mathbf{x})$ As explained in [2], solving (18) relies on the construction of a tangent model around the current iterate $\mathbf{x}$ that constitutes a quadratic first-order local approximation of the original problem. An adequate descent direction h in the $\mathbf{x}$-space is then computed by solving a convex quadratic program of the form

$$\min_{h\in\mathbb{R}^{q_\mathbf{x}}} \hat{f}_\infty(\mathbf{x}+h, \mathbf{x}) \triangleq \max_{(\phi,\Phi)\in\Xi} \phi - f_\infty(\mathbf{x}) + \Phi^T h + \frac{1}{2} h^T Q h \tag{19}$$

where, for a point $\mathbf{x}$, the set Ξ collects functions values $\phi \triangleq f(\mathbf{x}, \omega)$ and subgradients $\Phi \in \partial f(\mathbf{x}, \omega)$ over an extended set of frequencies $\overline{\Omega}$. Following [2], a sufficient requirement for the algorithm to converge, is that $\overline{\Omega}$ contains frequencies $\overline{\omega}$ that achieve the peak value in (18), i.e. $f_\infty(\mathbf{x}) = f(\overline{\omega}, \mathbf{x})$. This property ensures that the solution h in (19) is a descent direction of $f_\infty(\bullet)$ at the point $\mathbf{x}$. If $h = 0$, then $0 \in \partial f_\infty(\mathbf{x})$) and we are done. So, a stopping test can be formulated based on the solution to (19). A key fact about (19) is that the direction h can be used in an Armijo or Wolfe line search [5] which terminates after finitely many steps.

Note that in order to accelerate convergence, it is proposed in [1] to use a frequencies bracketing global maxima strategy, jointly with including frequencies corresponding to secondary peaks. Active and secondary peaks can easily be estimated using a method for the H_∞-norm computation, whereas bracketing frequencies can be computed using the Hamiltonian method [6].

Adding the constraints about the structure of F or its tunable parameters is handled through the introduction of a so-called progress function [3] which preserves both Clarke properties and the max structure in (18).

The resulting algorithm is guaranteed to converge to a critical point which is, unfortunately, a local minimum in practice, simply because the function $f_\infty(.)$ is non convex and thus, there is no guarantee to reach the global optimum. Furthermore, numerical difficulties may occur when Δ has a large numbers of repetitions k_i in parametric uncertainites $\delta_i^r I_{k_i}$, since the number of variables in the multipliers $\mathcal{M}_i$ increases. To overcome this problem, it is proposed in [10], two different algorithms. The first one is based on an inner relaxation technique, and the second one is based on a hybrid approach that treats real parametric δ_i^r and complex dynamic uncertainties Δ_i^C, individually. The interested reader can refer to [10] for more details.

3.3. A practical (expected) optimal approach

Theorem 1 is a convex formulation of the H_∞/H_- problem but may lead to a conservative solution as explained previously, whereas the nonsmooth technique converges to local optimal solutions, but it has the advantage to allow to fix extra constraints on F and to consider the nature and structure of the Δ block. Thus, and in order to take the benefit of the two techniques, the following practical procedure is proposed:

1) Solve the optimisation problem "$\min \gamma$ s.t. Eq. (10)-(12)" in order to obtain the global optimal solution M^*, F^*;

2) Performs a reduction of F^* using an adequate procedure, until a chosen order. It is preferred there a Grammian-based reduction approach, whose goal is to remove from F^*, small controllable and observable modes. Let us denote F_r the resulting reduced filter;

3) Inject M^*, F_r as the initial condition for the optimisation problem (18) and compute the (local) optimal solution M, F by solving (18).

By using this procedure, a reduced order fault detector F that fulfils all required performance can be obtained, expected to be close to the optimal performance provided by the full order solution M^*, F^*. Furthermore, since it solves the constraints (14) and (15) in spite of (7) and considers the nature and structure of Δ, a less conservative solution than M^*, F^* is obtained.

4. The μ_g analysis theory

The shortcomings of the theory developed in the previous section, are the formulation of the H_- constraint as a fictitious H_∞ requirement which involves a sufficient condition, and the non-smooth formulation which guarantees only a local optimal solution. To overcome these drawbacks, the so–called generalized structured singular value μ_g can be used as proposed in [24], see the notation section for the definition of μ_g.

The central result is theorem 6 in [24], which states that a *necessary and sufficient* condition for (3) and (4) to hold, is

$$\mu_{g\underline{\mathbf{\Delta}}}\left(\mathbf{N}(s)\right) < 1,\ \forall s = j\omega, \omega \in \Omega \tag{20}$$

with $\mathbf{\Delta} = diag(\Delta, \Delta_d, \Delta_f)$, where $\Delta_d \in \mathbb{C}^{q_d \times q}$ and $\Delta_f \in \mathbb{C}^{q_f \times q}$ are fictitious uncertainty blocks, referred as performance blocks. $\mathbf{N}$ is derived from G, K, W_d, W_f, M and F as illustrated on Fig. 3.

In other words, condition (20) provides a *necessary and sufficient* condition for the following design objectives, to hold:

$$\overline{\sigma}\left(T_{dr}(\Delta, j\omega)\right) \leq \overline{\sigma}\left(W_d(j\omega)\right) \quad \omega \in \mathbb{R} \cup \{\infty\},\ \Delta \in \mathbb{B}_\Delta \tag{21}$$

$$\text{and } \underline{\sigma}\left(T_{fr}(\Delta, j\omega)\right) \geq \underline{\sigma}\left(W_f(j\omega)\right) \quad \omega \in \Omega,\ \Delta \in \mathbb{B}_\Delta \tag{22}$$

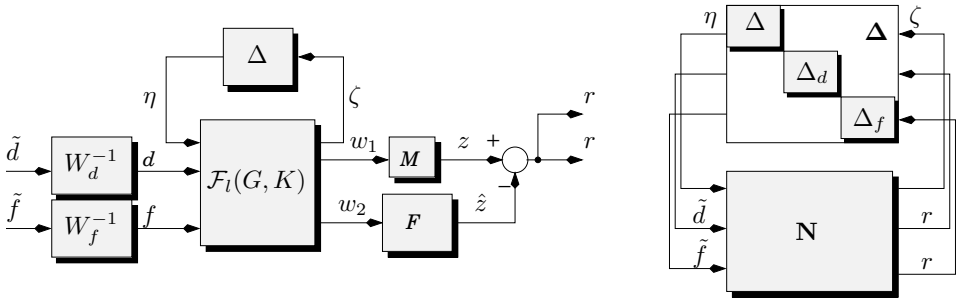

Figure 3: The μ_g formulation of the fault detection performance analysis problem

The goal of this section is to present recent developments within the μ_g-theory based on the aforementioned fundamental results, as a set of tools for robust performance assessment of the solution M, F derived from theorems 1 and 2, and more generally for any fault detector scheme whose performance within the H_∞/H_- framework, is under interest. Towards this end, we assume that the reader is familiar with the above results and we invite the reader, to look at the developments presented in [24, 25] for theoretical backgrounds, and [26, 21] for a good practice of this theory (to name a few papers).

The focus of the following sections is then as follows:

- First, we focus on the derivation of a sensitivity measure of μ_g against each component of its associated perturbation block, namely $\mathbf{\Delta} = diag(\Delta, \Delta_d, \Delta_f)$. We also call this measure *the μ_g-sensitivity functions*. With the definition of $\mathbf{\Delta}$, it is easy to see that the μ_g-sensitivity functions can quantify which uncertainty Δ_i, component of d and component of f, is the most responsible of the robust performance degradation of the fault detection scheme. Since μ_g is a frequency indicator, such an information will be given frequency by frequency (at frequencies for which μ_g will be evaluated, to be more precise).

- Second, the focus is on the derivation of performance indicators for worst-case performance analysis and margins. The idea is to identify, i) the combination of the uncertainties Δ_i that leads to fault detection performance loss and the frequencies at which it occurs, and ii),

the combination of the uncertainties Δ_i for which the performance margins are the biggest, and the frequencies at which it happens. Since elements of Δ are relative to e.g. physical parameters, time delays, etc. such measures can be used to determine the highest value of the parameter shift or time delay that can be inserted in the fault detection scheme, without losing the robust fault detection performance.

4.1. μ_g-sensitivity functions

It is well known that the sensitivity of a function with respect to a variable can be approached by the partial derivative of this function about the variable. Thus, it seems natural to use the following definition for the μ_g-sensitivity functions.

Definition 1. *Consider the structure $\mathbf{N}-\mathbf{\Delta}$ defined according to Fig. 3 (right). The μ_g sensitivity function $\mathcal{S}\mu_g^i(\omega_j)$ with respect to the ith element of $\mathbf{\Delta}$, is defined at a frequency ω_j according to:*

$$\mathcal{S}\mu_g^i(\omega_j) = \frac{\partial \mu_{g\underline{\mathbf{\Delta}}_i}(\mathbf{N}(s))}{\partial \mathbf{\Delta}_i} \quad s = j\omega_j \tag{23}$$

Except for special cases, μ_g is intractable and it is replaced by computable upper and lower bounds γ_{ub}, γ_{lb}. The lower bound γ_{lb} is computed using a similar algorithm to the power algorithm for μ [49]. The difference results in the Δ_f block (see Fig. 3) since it infers the $\underline{\sigma}$ function in spite of the $\overline{\sigma}$ function. For this block, a set of implicit equations are solved at each step of the standard power algorithm. With regards to the upper bound γ_{ub}, a LMI formulation is proposed in [33] by using the $D-G$ scaling matrices technique from the μ theory. The difference with the μ case, results in the real components of the D scaling matrices associated to Δ_f, since they are negative definite, highlighting the effect of the $\underline{\sigma}$ function (the H_- index). It follows that $\mathcal{S}\mu_g^i(\omega_j)$ is not computable in general. Then, $\mathcal{S}\mu_g^i(\omega_j)$ is approached by replacing μ_g in definition 1, by its upper and lower bounds γ_{ub} and γ_{lb}, i.e.

$$\frac{\partial \gamma_{lb}(\mathbf{\Delta}_i, \omega_j)}{\partial \mathbf{\Delta}_i} \leq \mathcal{S}\mu_g^i(\omega_j) \leq \frac{\partial \gamma_{ub}(\mathbf{\Delta}_i, \omega_j)}{\partial \mathbf{\Delta}_i} \tag{24}$$

The problem then turns out to be the computation of the partial derivative of the real valued univariate functions $\gamma_{lb}(\mathbf{\Delta}_i, \omega_j)$ and $\gamma_{ub}(\mathbf{\Delta}_i, \omega_j)$. This problem is solved here using the finite differences technique, and more precisely using the centered difference approach. This leads to the following proposition:

Proposition 1. *Consider the left and right terms in Eq. (24). Given a small value of $h > 0$ and an order of error $p \in \mathbb{Z}^+$,*

$$\frac{\partial g(\mathbf{\Delta}_i)}{\partial \mathbf{\Delta}_i} = \frac{1}{h} \sum_{k=k_m}^{k_M} C_k g(\mathbf{\Delta}_i + kh) + \mathcal{E}(h^p) \tag{25}$$

$$\text{with } \sum_{k=k_m}^{k_M} k^n C_k = \begin{cases} 0 & \text{for } n = 0, .., p, n \neq 1 \\ 1 & \text{if } n = 1 \end{cases}, \quad k_M = -k_m = \frac{p}{2}, \quad k, n \in \mathbb{Z} \tag{26}$$

for $g(\mathbf{\Delta}_i) = \{\gamma_{lb}(\mathbf{\Delta}_i, \omega_j), \gamma_{ub}(\mathbf{\Delta}_i, \omega_j)\}$. $\mathcal{E}(h^p)$ *refers to an error term, so that Eq.* (25) *becomes an approximation when omitting the term* $\mathcal{E}(h^p)$.

Proof: Direct application of the finite differences theory [36], considering the first order derivative problem and the centered difference approach. □

Note that Eq. (26) in proposition 1 defines a set of $p+1$ linear equations about $p+1$ unknown coefficients $C_k, k = k_m, ..., k_M$. Thus, a unique solution for all C_k can be easily computed using linear algebra, leading proposition 1 to be constructive to approximate numerically the μ_g-sensitivity functions $\mathcal{S}\mu_g^i(\omega_j)$.

Remark 3. *In almost all our studied applications,* $h = 1e^{-3}$ *and* $p = 4$ *has been revealed to be a suitable choice. This leads to the following definition for the parameters* $C_k, k = k_m, ..., k_M$*:* $C_{-2} = \frac{1}{12},\ C_{-1} = \frac{-2}{3},\ C_0 = 0,\ C_1 = \frac{2}{3},\ C_2 = \frac{-1}{12}$.

4.2. Worst-case performance analysis

The goal we pursue, is now to identify the combination of the elements of Δ that leads to fault detection performance loss, and the frequency at which it occurs. In this sense, such a couple (Δ, ω) corresponds to the worst-case for the fault detection scheme, so we refer this analysis to the worst-case performance analysis. Let us denote $(\Delta_{wc}, \omega_{wc})$ this couple. From (20), we know that such a situation occurs when $\mu_g \geq 1$, over $diag(\Delta_d, \Delta_f)$. So $\mu_g = 1$ over $diag(\Delta_d, \Delta_f)$, is the frontier of interest. This suggests the following definition for $(\Delta_{wc}, \omega_{wc})$.

Definition 2. *Consider the structure* $\mathbf{N} - \mathbf{\Delta}$ *illustrated on Fig. 3 (right). The worst uncertainty* Δ_{wc} *that takes its values in* $\mathbb{B}_\Delta$ *at the frequency* ω_{wc} *that belongs to a finite frequency range* $\mathbb{E}_\Omega$*, is defined according to:*

$$(\omega_{wc}, \Delta_{wc}) = \left\{(\omega, \Delta) : \mu_{g\breve{\underline{\Delta}}}\left(\mathcal{F}_u(\mathbf{N}(j\omega), \Delta)\right) = 1,\ \Delta \in \mathbb{B}_\Delta, \omega \in \mathbb{E}_\Omega\right\} \quad \Delta_{wc} \in \mathbb{B}_\Delta, \omega_{wc} \in \mathbb{E}_\Omega \quad (27)$$

where $\breve{\underline{\Delta}} = \{diag(\Delta_d, \Delta_f)\}$.

From definition 2, it follows that finding $(\Delta_{wc}, \omega_{wc})$ can be formulated according to the following optimisation problem

$$\begin{aligned}(\Delta_{wc}, \omega_{wc}) = &\text{argmin } \left|\mu_{g\breve{\underline{\Delta}}}\left(\mathcal{F}_u(\mathbf{N}(j\omega), \Delta)\right) - 1\right| \\ &\text{s.t. } \Delta \in \mathbb{B}_\Delta,\ \ \omega \in \mathbb{E}_\Omega\end{aligned} \quad (28)$$

Remark 4. *Note that as stated by definition 2, the couple* $(\omega_{wc}, \Delta_{wc})$ *is not necessarily unique, so that it is required to find all solutions* $(\omega_{wc}, \Delta_{wc})$*. This problem can be solved by running the optimisation problem* (28) *as many time as necessary, on* a priori *chosen frequency ranges* $\mathbb{E}_\Omega$*. In other words, when the solution* $(\omega_{wc}, \Delta_{wc})$ *is not unique and thus global, local solutions can be found by tuning the lower and upper bounds of the constraint about* ω*, in the optimisation problem* (28)*. The frequency plot of* $\mu_{g\breve{\underline{\Delta}}}(\mathbf{N}(j\omega))$ *can help to select judiciously these bounds, see section 5 that presents an illustration.*

To solve the optimization problem (28), the recent particle swarm optimization (PSO) algorithm proposed in [43], is considered. PSO technique is useful since it does not require any gradient

information and is suitable for discontinuous optimization problems [28, 32, 35]. The principle of the PSO technique consists in finding optimal regions of search spaces through random movements of individuals in a population (swarm) composed of particles. Each particle is characterized by its position and its velocity, the position of a particle representing a solution of the search space and thus, a possible solution of the optimization problem. The central ingredient of a PSO algorithm is the equations that update the velocity and the position of each particle. Due to weak exploration ability of basic versions of PSO algorithms [28, 32, 35], local solutions may be found. To overcome this shortcoming, it is proposed in [43] a velocity update equation with a location abandoned mechanism based on an exponential function.

Here, we use the same principle. The difference between the proposed PSO algorithm and the one given in [43], consists of a particular choice of the so–called inertia weight involved in the velocity update equations, that shares the same structure than the location abandonned mechanism. More precisely, it is based on a rationnal polynomial function in spite of an exponential one. This has been revealed to be numerically more suitable for our problem. Towards this end, the following developments focus on the main steps of the proposed PSO algorithm and we invite the interested reader to refer to [43] for necessary backgrounds.

To proceed, consider the optimisation problem (28) and let us gather Δ and ω into a unique vector $\mathbf{x} \in \mathbb{E}_{\mathbf{x}} = [\underline{\mathbf{x}}, \overline{\mathbf{x}}] \subset \mathbb{R}^{q_{\mathrm{x}}}$, where $\underline{\mathbf{x}}$ and $\overline{\mathbf{x}}$ refers to lower and upper bounds of constraints, and q_{x} the dimension of the search space. Then, the optimisation problem (28) can be reformulated according to the general form

$$\begin{array}{l} \min\ f(\mathbf{x}) \\ s.t.\ \mathbf{x} \in \mathbb{E}_{\mathbf{x}} = [\underline{\mathbf{x}}, \overline{\mathbf{x}}] \subset \mathbb{R}^{q_{\mathrm{x}}} \end{array} \tag{29}$$

where $f(\mathbf{x}) = \left| \mu_{g\underline{\check{\Delta}}} \left(\mathcal{F}_u(\mathbf{N}(j\omega), \Delta) \right) - 1 \right| : \mathbb{E}_{\mathbf{x}} \to \mathbb{R}^+$, is a real-valued function. Let us denote the position and the velocity of the particle i at the iteration k as $\mathbf{x}_i(k) = \left(\mathrm{x}_i^1(k), ..., \mathrm{x}_i^{q_{\mathrm{x}}}(k) \right)$ and $\mathbf{v}_i(k) = \left(\mathrm{v}_i^1(k), ..., \mathrm{v}_i^{q_{\mathrm{x}}}(k) \right)$, respectively. Following the developments presented in [43], the position of each particle is updated by using the following equations

$$\begin{array}{l} \mathbf{V}_1 = \chi(k)\mathbf{v}_i(k) + c_1 r_1 (\mathbf{p}_i^*(k) - \mathbf{x}_i(k)) \\ \mathbf{V}_2 = \chi(k)\mathbf{v}_i(k) + c_2 r_2 (\mathbf{g}_i^*(k) - \mathbf{x}_i(k)) \\ \mathbf{V}_3 = \chi(k)\mathbf{v}_i(k) + c_1 r_1 (\mathbf{p}_i^*(k) - \mathbf{x}_i(k)) + c_2 r_2 (\mathbf{g}_i^*(k) - \mathbf{x}_i(k)) \\ \mathbf{v}_i(k+1) = \{ \mathbf{V}_j = \mathrm{argmin} \{ f(\mathbf{x}_i(k) + \mathbf{V}_j) \}, j = 1, 2, 3 \} \\ \mathbf{x}_i(k+1) = \mathbf{x}_i(k) + \mathbf{v}_i(k+1) \end{array} \tag{30}$$

where r_1 and r_2 are random number in $[0, 1]$. c_1 and c_2 are the so–called cognitive and social coefficients, respectively. $\mathbf{p}_i^*$ and $\mathbf{g}_i^*$ are the historical optimal position of the particle i and the best position among all particles, respectively. $\chi(k)$ is the inertia weight, that must be selected to be a decreasing function in k. Here, the following expression is retained for the inertia weight $\chi(k)$

$$\chi(k) = \underline{\chi} + \left(\overline{\chi} - \underline{\chi} \right) \frac{1}{1 + k^{q_{\chi}}} \tag{31}$$

where $\underline{\chi}, \overline{\chi}$ denote the minimum and maximum inertia weight. The parameter $q_\chi > 1$ enables to fix the decreasing speed of $\chi(k)$. Now, assume that a particle stays at a given position during a certain number of movements q_L, which is understood in the optimisation process as a local optimal position. Then, by virtue of the following equation, a new position of the particle with a small probability, is generated in the search space

$$\mathbf{x}_{i_{new}} = \begin{cases} (1-\chi(k))\mathbf{g}^*(k) + \rho_1 \frac{1}{1+k^{q_\chi}}(\mathbf{g}^*(k) - \mathbf{x}_i(k)) & \text{if } r < 0.99 \\ \underline{\mathbf{x}}_i + \rho_2.(\overline{\mathbf{x}}_i - \underline{\mathbf{x}}_i) & \text{else} \end{cases} \tag{32}$$

where r and $\rho_i, i = 1, 2$ are random numbers in $[0, 1]$ and $[-1, 1]$, respectively. The pseudo code of the proposed PSO algorithm is the one given by Algorithm 1 in [43] by considering Eqs. (30)-(32). It is recalled in the appendix for convenience, see Algorithm 2.

Remark 5. *It can be seen from Eq.* (30) *to* (32)*, that the parameters that control the PSO algorithm, i.e. the parameters that have to be chosen by the user, are the population size p_s and the coefficients $c_1, c_2, \underline{\chi}, \overline{\chi}, q_\chi, q_L$. Following our experience, $p_s = 30, c_1 = 0.5, c_2 = 1.25, \underline{\chi} = 0.9, \overline{\chi} = 1.3, q_\chi = q_L = 3$ has been revealed to be a suitable choice, to solve efficiently the optimisation problem* (28)*.*

4.3. Performance margins

The last μ_g-based performance criteria that is proposed, consists in identifying the combination of the elements of Δ that leads the performance margins to be the biggest, and the frequency at which it happens, so we refer this analysis to the performance margins. Let us denote (Δ_m, ω_m) this couple. From (20), we know that such a situation occurs when μ_g takes its minimal value, over $\breve{\Delta} = diag(\Delta_d, \Delta_f)$. So $\min \mu_g$ over $\breve{\Delta}$ is the case of interest. This suggests the following definition for (Δ_m, ω_m).

Definition 3. *Consider the structure $\mathbf{N} - \mathbf{\Delta}$ illustrated on Fig. 3 (right). The uncertainty Δ_m that takes its values in $\mathbb{B}_\Delta$ at the frequency ω_m that belongs to a finite frequency range $\mathbb{E}_\Omega$, is defined according to:*

$$\begin{aligned} (\omega_m, \Delta_m) = &\text{argmin } \mu_{g\underline{\breve{\Delta}}}\left(\mathcal{F}_u(\mathbf{N}(j\omega), \Delta)\right) \\ &\text{s.t. } \Delta \in \mathbb{B}_\Delta, \omega \in \mathbb{E}_\Omega \end{aligned} \tag{33}$$

Definition 3 is clearly an optimisation problem over $\Delta \in \mathbb{B}_\Delta$ and $\omega \in \mathbb{E}_\Omega$, that can be solved using the PSO algorithm 2, proposed previously. For that purpose, Δ and ω are gathered into $\mathbf{x} \in \mathbb{E}_\mathbf{x} = [\underline{\mathbf{x}}, \overline{\mathbf{x}}] \subset \mathbb{R}^{q_\mathbf{x}}$, where $\underline{\mathbf{x}}$ and $\overline{\mathbf{x}}$ refers to lower and upper bounds of constraints, and the optimisation problem (33) is formulated according to the general form given by Eq. (29) with $f(\mathbf{x}) = \mu_{g\underline{\breve{\Delta}}}\left(\mathcal{F}_u(\mathbf{N}(j\omega), \Delta)\right) : \mathbb{E}_\mathbf{x} \to \mathbb{R}^+$.

Remark 6. *Note that as opposed to the worst-case performance analysis problem, the solution (ω_m, Δ_m) is unique, since we look for the minimal value of $\mu_{g\underline{\breve{\Delta}}}\left(\mathcal{F}_u(\mathbf{N}(j\omega), \Delta)\right)$ over $\mathbb{E}_\Omega$.*

5. Application to a satellite mission

The $H_\infty/H_-/\mu_g$ theory developed in the above sections, is now considered to address the problem of fault diagnosis in the thruster–based propulsion unit of a satellite. For easy reference, we recall that the methodology results in the main steps described by algorithm 1.

Algorithm 1 Main steps of the $H_\infty/H_-/\mu_g$ design/analysis methodology

1: Establish the satellite's dynamics together with the fault models, the uncertainties and the control architecture
2: Define the performance objective functions $W_d(s)$ and $W_f(s)$
3: Solve the LMI optimization problem defined by equations (10),(11),(12). This leads to the global solution (M^*, F^*).
4: Perform an order reduction of F^* to the desired order. This leads to a reduced solution (M^*, F_r).
5: Use (M^*, F_r) as the initial condition of the non-convex optimization problem (18) and compute the (local) optimal solution (M, F).
6: Analyse the so-derived solution using the set of μ_g tools, i.e. the frequency dependent μ_g function (20), the μ_g-sensitivities (23), the worst-case performance criteria (27) and the performance margins (33), to go deeper insight into the obtained solution.
7: If the μ_g analysis leads to unsatisfactory performance, go to step 2 and refine $W_d(s)$ and $W_f(s)$ until an optimal solution is found. Find a trade-off between $W_d(s)$ and $W_f(s)$ following the Paretto principle, if necessary.

The satelite's reference scenario is inspired by the one considered in [37]. It consists of a satellite that performs a so-called orbit restitution manoeuvre around Earth, i.e. the satellite performs a translation from a given position to a reference orbit, while maintaining its attitude constant. It is assumed that the satellite is equipped by a large solar array, that causes flexible motions.

Recent studies demonstrate that the problem of thruster fault diagnosis in satellites, can be completely solved considering the satellite's attitude [15, 37, 9]. Thus, the following restricts the discussion to the satellite's attitude, even if the full mission, and thus the simulator used to derive the results presented in this paper, also considers both the translational and rotational motions.

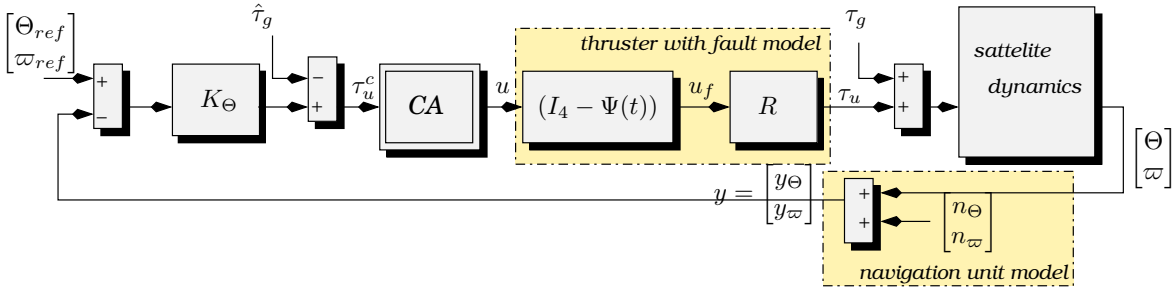

Figure 4: Diagram of the satellite attitude control loop

Fig. 4 illustrates the attitude's loop. In terms of avionics, a star tracker and an inertial measurement unit equip the satellite, so that both the attitude angles $\Theta = [\phi\ \theta\ \psi]^T$ and the angular

rates $\varpi = [p\ q\ r]^T$ given in the so-called body frame, are assumed to be estimated by the navigation unit. Decorrelated band-limited normally distributed white noises passing through high pass filters with cutting frequency equal to $1rd/s$, are assumed to model the estimation errors, denoted n_Θ and n_ϖ in Fig 4. In terms of actuators, a set of four thrusters of $1N$ also equips the satellite. The attitude's control unit consists of a multivariable PID–like controller and a feedforward loop, that computes the torque command signal $\tau_u^c \in \mathbb{R}^3$ so that:

$$\tau_u^c(s) = K_\Theta(s)\left[\varepsilon_\Theta(s)^T\ \varepsilon_\varpi(s)^T\right]^T - \hat{\tau}_g(s) \tag{34}$$

In this equation, ε_Θ and ε_ϖ refer to the attitude and angular rates tracking errors. $\hat{\tau}_g \in \mathbb{R}^3$ refers to the feedforward loop, that consists of an estimation of environmental disturbances torque caused by gravity gradient, Earth magnetic field, atmospheric drag and solar pressure (denoted τ_g on Fig. 4). τ_u^c is then converted to the unidirectional thruster control signals u, by means of a control allocation algorithm, see Fig. 4 that indicates the location of the control allocation unit (denoted CA). Finally, in terms of reference trajectory, since it is required to maintain the attitude to zero, $\Theta_{ref} = 0$ and $\varpi_{ref} = 0$.

5.1. Modelling issues

The rotational motion of the satellite can be derived from the Euler's second law in the body frame, i.e.:

$$\dot{\varpi} = J^{-1}\left(\sum_k \tau_k - \varpi \times J\varpi\right) \tag{35}$$

Here, $J \in \mathbb{R}^{3\times3}$ is the inertia matrix of the satllite without considering the solar array. In (35), $\sum_k \tau_k \in \mathbb{R}^3 = \tau_u + \tau_g + \tau_{sa}$ describes the sum of torques about the satellite's CoM, in the body frame. The (endogenous) torque $\tau_{sa} \in \mathbb{R}^3$ is caused by the solar array dynamics, that are given by the following vector-based equations

$$\ddot{\bar{q}} + 2\xi\omega_0\dot{\bar{q}} + \omega_0^2\bar{q} = -L^T\dot{\varpi} \quad \bar{q} \in \mathbb{R}^{n_s.n_p} \tag{36}$$

$$\tau_{sa} = -k\left(L\ddot{\bar{q}} + J_{sa}\dot{\varpi}\right) \tag{37}$$

$$L = \mathcal{R}(\beta)B_R \in \mathbb{R}^{3\times(n_s.n_p)} \tag{38}$$

In these equations, $n_p = 1$ is the number of solar arrays and $n_s = 2$ is the number of flexible modes per solar array. ξ, ω_0, B_R refer to damping factors, frequencies and participation matrices of flexible modes. J_{sa} refers to the inertia matrix of the solar array, and $\mathcal{R}(\beta)$ is a rotation matrix in charge to transform B_R given in the solar array frame, into the satellite's body frame. In this work, β is considered constant since the solar array is considered to be immobile. k is a dimensionless paramter that enables to scale τ_{sa}. The numerical values of the parameters are given in appendix, see table B.4.

Finally, using the individual rotation matrices from Euler (3,2,1) rotation, the relationship between ϖ and the rate of the Euler angles Θ is given by:

$$\dot{\Theta} = \frac{1}{\cos(\theta)}\begin{bmatrix}\cos(\theta) & \sin(\phi)\sin(\theta) & \cos(\phi)\sin(\theta)\\ 0 & \cos(\phi)\cos(\theta) & -\sin(\phi)\cos(\theta)\\ 0 & \sin(\phi) & \cos(\phi)\end{bmatrix}\varpi \tag{39}$$

Now, let $R \in \mathbb{R}^{3\times4}$ be the thruster configuration matrix, see the appendix for numerical values. Then, $\tau_u = Ru$. Combining Eq. (35)-(39) leads to a nonlinear state space model of satellite's attitude, so that

$$\begin{aligned}\dot{x} &= f(x) + B_\tau R u + B_\tau \tau_g \\ &= f(x) + Bu + B_\tau \tau_g \end{aligned} \tag{40}$$

$$y = \begin{bmatrix} I_6 & 0_{6\times4}\end{bmatrix} x + [n_\Theta^T \; n_\varpi^T]^T \tag{41}$$

with the state vector $x = [\Theta^T \; \varpi^T \; \bar{q}^T \; \dot{\bar{q}}^T]^T \in \mathbb{R}^{10}$, the (noisy) measurements $y = [y_\Theta^T \; y_\varpi^T]^T = [(\Theta + n_\Theta)^T \; (\varpi + n_\varpi)^T]^T \in \mathbb{R}^6$ being provided by the navigation unit, as explained previously.

With regards to the faults, the mathematical model proposed in [19] is retained, i.e. the real status of the thrusters at the time t, which is of course unknown, is modelled as $u_f(t) = (I_4 - \Psi(t))\, u(t)$, with $\Psi(t) = diag\,(\psi_1(t), ..., \psi_4(t))$, where $0 \leq \psi_i(t) \leq 1, i = \overline{1,4}$ are unknown. The index "f" refers to a faulty status. By using such a formulation, $\psi_i(t) = 0, \forall i$ indicates that all thrusters have a normal functioning, whereas $\psi_i(t) = 1 - \phi_i(t)/u_i(t)$ with a suitable expression for $\phi_i(t)$, indicates that the ith thruster is faulty, with some time profile. Typically, $\phi_i(t) = \max\{u_i(t), 1\}$ corresponds to the ith thruster being fully opened (stuck-open fault case), whereas $\phi_i(t) = 0$ corresponds to the ith thruster being closed (stuck-closed fault case).

Then, performing a first order Taylor approximation of the nonlinear function $f(x)$ around $x = 0$, and applying the fault modelling approach proposed in [19], the satellite attitude dynamic is described by

$$\dot{x} = Ax + Bu + B_\tau \tau_g + \sum_{i=1}^{4} H_i f_i \tag{42}$$

$$y = \begin{bmatrix} I_6 & 0_{6\times4}\end{bmatrix} x + [n_\Theta^T \; n_\varpi^T]^T \tag{43}$$

where the i^{th} column of the matrix H is the i^{th} fault signature associated to the i^{th} fault mode f_i. The indices $i = \overline{1,4}$ also coincide with the numbering of thrusters, and thus with the columns of the matrix R.

Of course, some parameters of this model are partially known, namely the satellite inertia matrix J, the solar array inertia matrix J_{sa}, the damping factors ξ and frequencies ω_0 of the flexible modes characterizing the solar array, see table B.4. So Eq. (42)-(43) defines an uncertain state space model. Thus, it is put into a LFT form, which leads to:

$$y(s) = \mathcal{F}_u(P_u(s), \Delta) \begin{bmatrix} \tau_g(s) \\ f(s) \\ u(s) \end{bmatrix} + \begin{bmatrix} n_\Theta(s) \\ n_\varpi(s) \end{bmatrix} \tag{44}$$

$$\Delta = diag\left(\delta_{J_{xx}} I_8, \delta_{J_{sa_{xx}}} I_8, \delta_{J_{yy}} I_{18}, \delta_{J_{sa_{yy}}} I_{18}, \delta_{J_{zz}} I_{18}, \delta_{J_{sa_{zz}}} I_{18}, \delta_{\xi_1} I_2, \delta_{\xi_2} I_3, \delta_{\omega_{0_1}} I_2, \delta_{\omega_{0_2}} I_3\right),\ \Delta \in \mathbb{R}^{98\times98} \tag{45}$$

In other words, all uncertain parameters entering in (42) are "pulled out" so that the model appears

as a LTI nominal model P_u subject to an artificial block diagonal Δ specifying how each uncertainty enters P_u, see [8, 18] for instance. In this formalism, the uncertainties entering in (44) have been scaled, so that $|\delta_\bullet| \leq 1 \Leftrightarrow \Delta \in \mathbb{B}_\Delta$.

5.2. Direct application of the theory

The goal we pursue now, is to design a H_∞/H_- residual generator, able to robustly detect stuck-open and stuck-closed faults, that may occur in a thruster. Following the developments stated in section 2, let us define w_1, w_2 and q according to

$$w_1 = \begin{bmatrix} y_\Theta \\ u \end{bmatrix} \quad w_2 = \begin{bmatrix} y_\varpi \\ u \end{bmatrix} \quad q = 1 \tag{46}$$

Note that with the choice $q = 1$, we seek for a residual r of dimension "1". This choice is motivated by the fact that, here, only the fault detection problem is considered. In other words, a fault indicating signal r of dimension "1" is expected to be enough to robustly detect any kind of faults occurring in any thruster.

Then, the LFT model $\mathcal{F}_u(G, \Delta)$ illustrated on Fig. 1 is derived from the setup illustrated on Fig. 4 and from $\mathcal{F}_u(P_u, \Delta)$, by means of state-space algebra. Δ is defined by Eq. (45), $d = \left[n_\Theta^T \, n_\varpi^T\right]^T$, and the controller K is defined according to $K = R^+ K_\Theta$, $R^+ : RR^+ = I$ being any inverse of the thruster configuration matrix R, which models the control allocation unit, see [14] for a discussion on modelling a control allocation unit. The problem dimensions are thus

$$q_\eta = q_\zeta = 98,\ q_d = 6,\ q_f = 4,\ m_1 = m_2 = 7,\ q = 1$$

Next and as explained in section 3, the robustness requirements against d and fault sensitivity objectives against f must be specified through the adequate choice of W_d and W_f. Here, d refers to attitude and angular rates measurement errors, that are modelled as decorrelated white noise passing trough former filters having cutting frequency at $1rd/s$. Thus, it seems natural to choose W_d as a diagonal transfer of six low pass filters with cutting frequency $\omega_d = 1rd/s$, that is

$$W_d(s) = diag\left(\gamma_\Theta \frac{1 + s/\omega_{hf}}{1 + s/\omega_d} I_3, \gamma_\varpi \frac{1 + s/\omega_{hf}}{1 + s/\omega_d} I_3\right) \quad \omega_d = 1rd/s,\ \omega_{hf} >> \omega_d \tag{47}$$

with γ_Θ and γ_ϖ the smallest as possible. By such a choice, it is required to attenuate the attitude and angular rates measurement errors on the residual r, the most possible, with a particular attention in the frequency range $[1rd/s, +\infty[$. ω_{hf} is a frequency introduced to make W_d invertible.

With regards to the fault sensitivity objective, it is required for r to be as sensitive as possible to all faults $f_i, i = 1, ..., 4$, from $0rd/s$ up to the highest possible frequency, with the highest magnitude possible. Then, W_f is chosen as a diagonal transfer of four low pass filters with cutting frequency ω_f, that is

$$W_f(s) = diag\left(\gamma_{f_1} \frac{1 + s/\omega_{hf}}{1 + s/\omega_f}, ..., \gamma_{f_4} \frac{1 + s/\omega_{hf}}{1 + s/\omega_f}\right) \quad \omega_{hf} >> \omega_f \tag{48}$$

with $\gamma_{f_i}, i = 1, .., 4$ and ω_f as large as possible. The gains $\gamma_{f_i}, i = 1, .., 4$ of the elements of W_f are introduced to manage the sensitivity to faults $f_i, i = 1, ..., 4$ separately, and ω_{hf} is introduced to

make W_f invertible.

The full order global optimal solution (M^*, F^*) is then computed following the theory explained in section 3.1. The parameters $\gamma_\Theta,\ \gamma_\varpi,\ \gamma_{f_i}, i = 1, ..., 4,\ \omega_f$ are determined through an iterative refinement, such that the μ_g-analysis procedure (i.e. condition (20)) leads a μ_g value close to "1" per lower value, for the highest frequency range as possible. This indicates that the best robustness and fault sensitivity performance have been achieved. This boils down the following optimal values for $\gamma_\Theta,\ \gamma_\varpi,\ \gamma_{f_i}, i = 1, ..., 4,\ \omega_f$, with a filter F^* of order $n_F = 16$.

$$\gamma_\Theta = 0.1,\ \gamma_\varpi = 1,\ \gamma_{f_1} \approx 0.0105,\ \gamma_{f_2} \approx 0.0711,\ \gamma_{f_3} \approx 0.003,\ \gamma_{f_4} \approx 0.082,\ \omega_f = 0.1rd/s$$

Next, and as explained in section 3.3, a Grammian-based reduction procedure is applied to F^*, in order to obtain a reduced order filter F_r of order 7. M^* and F_r are then passed as an initial condition, to the non smooth design approach presented in section 3.2, and the final solution (M, F) is then deduced from theorem 2. Fig. 5 and Fig. 6 illustrate the sigma plots of $T_{n_\Theta r}(j\omega)$, $T_{n_\varpi r}(j\omega)$ and $T_{f_i r}(j\omega), i = 1, ..., 4$ for some *a priori* fixed values of Δ given by (45), for the two solutions (M^*, F^*) and (M, F). From these figures, we argue that the local solution (M, F) derived from the non smooth formulation (17), is close to the global optimal solution (M^*, F^*) derived from the LMIs (10)-(12). However, the benefit is that F is of reduced order (F is of order 7), as opposed to F^* which is of order 16.

The μ_g tools presented in section 4, are next used to assess and quantify the robust performance of the solution (M, F). The μ_g function $\mu_{g\underline{\mathbf{\Delta}}}(\mathbf{N}(j\omega))$ is first computed with respect to $f_i, i = 1, ..., 4$, see Fig. 7. The μ_g-sensitivities $\mathcal{S}\mu_g^i(\omega)$ are next evaluated, following the theory presented in section 4.1, see Fig. 8. The worst-case performance and the performance margins analyses presented in sections 4.2 and 4.3, are presented in tables 1 and 2.

As it can be seen, $\mu_{g\underline{\mathbf{\Delta}}}(\mathbf{N}(j\omega)) < 1$ in the frequency range $\Omega \approx [0; 0.1]rad/s$, which definitively demonstrates by virtue of Eqs. (21)-(22), that both the robustness requirement against the measurement errors n_Θ and n_ϖ specified by W_d and the fault sensitivity objectives imposed by W_f, are achieved for all uncertainties listed in table B.4. From the μ_g-sensitivities plots, it can be concluded that the residual r is most sensitive to disturbances and faults, than the rest of the uncertainties. Furthermore, and not surprisingly, it can be seen how r is sensitive to the two flexible modes of the solar array. There is however an interesting phenomenon that can be noticed for the case of faults in thruster n. 3: the sensitivity of r against the components J_{yy} and J_{zz} of the satellite inertia matrix, is similar to those of the measurement errors and the fault, see Fig. 8 left bottom. From tables 1 and 2, we can see that, for all faults, the worst case combination of uncertainties that leads to performance loss, occurs at $\omega_{wc} \approx [0.1; 0.4]rd/s$ and that the highest performance margins occur for $\omega_m \to 0rd/s$ except for f_3 where $\omega_m \approx 0.0387rd/s$, which is coherent with the μ_g plot illustrated on Fig. 7.

The fault detector (M, F) is finally implemented within the nonlinear simulator of the satellite's mission. In order to have a well numerically conditioning fault detector, the balanced input/output realization of (M, F) is computed and the resulting state-space realization is next converted into its discrete time form, by means of the Tustin transformation. This allows to have a solution ready to be implemented in a real processing unit, with some prior validation certificates obtained through a simulation environment. Fig. 9 illustrates the results for stuck-open faults (Fig.9.left) and stuck-closed faults (Fig.9.right), all occurring at $t = 100s$. Clearly, it can be seen that all faults

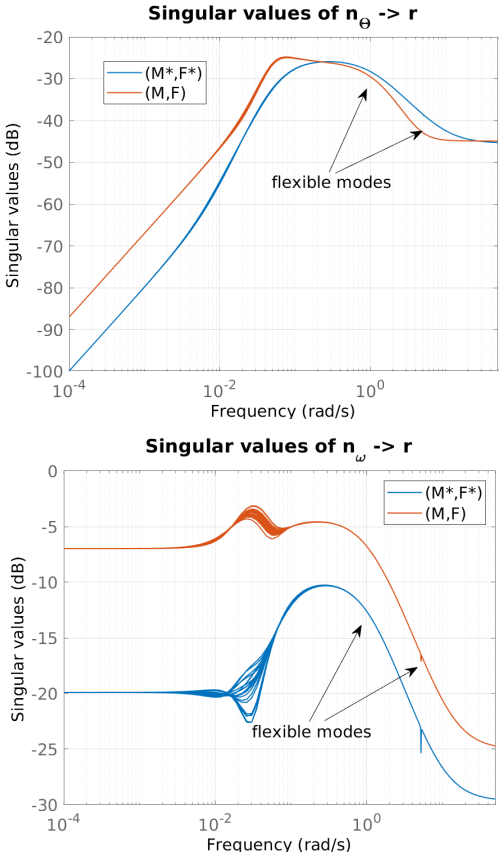

Figure 5: Sigma plots of $T_{n_\Theta r}(j\omega)$ (left) and $T_{n_\varpi r}(j\omega)$ (right)

can be detected successfully, using e.g. a simple threshold-based decision making rule or a more sophisticated test like the mean/variance Generalized Likelihood Ratio tests [4].

5.3. $H_\infty/H_-/\mu_g$ as a general theory

In this last section, we would like to demonstrate, how generic are the H_∞/H_- and the μ_g theories presented in this paper. Thus, we consider three different fault detection schemes and demonstrate how the tools presented in this paper, can be used to analyse, improve and complete, existing solutions in the FDI literature. It should be outlined that, even if all tools are applicable to all presented examples, we do not consider all of them, for brevity reasons. Here, the objective is to give a short, but exhaustive, panorama of the potential of the theories presented in this paper. Towards this end, section 5.3.1 considers the worst case performance and margins analysis with an unknown input observer fault diagnosis scheme. Section 5.3.2 is devoted to the μ_g-sensitivity analysis for a Kalman–based fault estimator scheme and section 5.3.3 demonstrates how the non-smooth H_∞/H_- design methodology can be used to enhance fault detection performance of an existing FDI scheme.

	Δ_{wc}										ω_{wc}
	J_{xx}	J_{yy}	J_{zz}	$J_{sa_{xx}}$	$J_{sa_{yy}}$	$J_{sa_{zz}}$	ξ_1	ξ_2	ω_{0_1}	ω_{0_2}	
f_1	14.9383	10.6216	12.4573	0.9718	19.4946	10.1206	0.0026	0.0031	1.0107	4.4993	0.3370
f_2	14.1055	9.4456	12.5261	0.9678	20.2635	10.9298	0.0033	0.0028	1.1511	5.3454	0.1401
f_3	14.4899	9.4555	13.7859	1.0288	19.3980	10.4281	0.0030	0.0031	1.0369	4.6080	0.4536
f_4	14.9466	9.6188	13.2621	1.0410	19.7267	9.2001	0.0031	0.0027	0.9746	5.3467	0.1529

Table 1: Worst case performance analysis

	Δ_m										ω_m
	J_{xx}	J_{yy}	J_{zz}	$J_{sa_{xx}}$	$J_{sa_{yy}}$	$J_{sa_{zz}}$	ξ_1	ξ_2	ω_{0_1}	ω_{0_2}	
f_1	13.5396	10.7687	14.0973	1.0189	17.5283	9.9630	0.0032	0.0030	1.0441	4.8029	0.0000
f_2	13.5949	10.1398	12.5485	1.0178	18.5988	10.1517	0.0031	0.0028	1.1619	4.8634	0.0000
f_3	12.6000	10.0392	14.3000	0.9513	17.1000	9.8528	0.0033	0.0028	0.9342	4.7772	0.0387
f_4	14.7663	9.3549	13.6642	0.9371	18.6778	9.6417	0.0033	0.0027	1.1769	4.7582	0.0000

Table 2: Performance margin analysis

5.3.1. Unknown Input Observer–based scheme

Assume that a set of four LTI unknown input observers (UIOs) has been designed for fault isolation, such that a given estimation error, say the ith estimation error $e_i \in \mathbb{R}^3$ defined by $e_i = \varpi - \hat{\varpi}$, is decoupled from f_i, while remaining sensitive to the three others. Thus, fault isolation is performed at each time t, by seeking which $||e_i(t)||_2$ is minimal at each t. We assume that the UIOs have been designed, e.g. using the method presented in [23], so that the total FDI solution results of the four signals $e_i, i = 1, ..., 4$ for fault isolation, and a say, a "robustified" residual $r = We = W[...e_i^T...]^T, i = 1, ..., 4 : e \in \mathbb{R}^{12}$, where $W \in \mathbb{R}^{1\times 12}$ is calculated as the solution of the minimisation problem min $\frac{||T_{dr}(0)||_2}{||T_{fr}(0)||_2}$.

The goal we pursue is to evaluate the robust performance of r against the uncertainties listed in table B.4, in the H_∞/H_- criteria sense. We argue that μ_g-tools can be used for that purpose. To proceed, consider the scheme illustrated on Fig. 10, which is deduced from Fig. 4 by inserting the four UIOs and the matrix W. With $\mathcal{F}_u(P_u(s), \Delta)$ given by (44)-(45) as the model of the satellite dynamics and the additive fault model of the thruster faults, $\mathbf{N}$ is constructed as illustrated on Fig.3.right. With regards to the objective functions W_d and W_f, we obtained:

$$\gamma_\Theta = 0.1,\ \gamma_\varpi = 10,\ \gamma_{f_1} \approx 0.0015,\ \gamma_{f_2} \approx 0.0123,\ \gamma_{f_3} \approx 0.01,\ \gamma_{f_4} \approx 0.0108,\ \omega_f = 0.1rd/s$$

The μ_g-based criteria are presented in Table 3. From these results, we argue that the UIO-based scheme has smaller performance than those of the H_∞/H_- fault detector calculated in the previous section, since:

- the gain γ_ϖ that enters in W_d is ten times bigger than in the case of the H_∞/H_- fault detector. This means that the navigation errors $n_\varpi(t)$ related to angular velocities will be amplified on $r(t)$, ten times more than in the case of the H_∞/H_- filter;
- except for γ_{f_3}, the gains $\gamma_{f_i}, i = 1, 2, 4$ that enter in W_f are much more smaller than in the

case of the H_∞/H_- fault detector. This means that $r(t)$ will have a less sensitivity level against faults in thrusters $1, 2, 4$ than in the case of the H_∞/H_- fault detection unit.

	Δ_{wc}										
	J_{xx}	J_{yy}	J_{zz}	$J_{sa_{xx}}$	$J_{sa_{yy}}$	$J_{sa_{zz}}$	ξ_1	ξ_2	ω_{0_1}	ω_{0_2}	ω_{wc}
f_1	12.9924	9.9767	12.4585	1.0631	20.8263	10.1629	0.0027	0.0033	0.9092	5.7054	0.2601
f_2	14.7577	10.2887	12.5945	0.9977	18.9860	10.5152	0.0030	0.0029	0.8473	5.2208	0.2810
f_3	14.3157	10.5102	12.9891	1.0172	20.6165	9.6196	0.0032	0.0034	1.0389	5.0198	0.2126
f_4	13.8822	10.5749	12.2182	0.9709	17.7627	9.4148	0.0035	0.0032	0.8171	5.6733	0.4517

	Δ_m										
	J_{xx}	J_{yy}	J_{zz}	$J_{sa_{xx}}$	$J_{sa_{yy}}$	$J_{sa_{zz}}$	ξ_1	ξ_2	ω_{0_1}	ω_{0_2}	ω_m
f_1	15.4000	10.9964	14.3000	1.0069	17.1000	9.6683	0.0034	0.0029	0.8508	4.4863	0.0850
f_2	12.6000	9.4735	11.7000	1.0632	17.1000	9.0001	0.0032	0.0029	1.1090	4.9972	0.0753
f_3	12.6000	9.0000	14.3000	0.9516	17.1000	9.2069	0.0034	0.0025	1.0026	4.5007	0.0786
f_4	15.4000	9.9349	11.7000	0.9004	17.1000	9.0008	0.0033	0.0029	1.0107	5.6394	0.0790

Table 3: Performance criteria for the UIOs-based scheme

This analysis is confirmed by nonlinear simulations, see Fig.13.left. Comparing with Fig. 9, it is interesting to note that, *i)* first, the UIO-based residual r is approximatively ten times of less magnitude than the H_∞/H_--based residual as predicted by the μ_g analysis, *ii)* second, the UIO-based residual is more sensitive to the flexible modes than the H_∞/H_--based residual, as it is predicted by the μ_g tools. Finally, note that the performance of the UIOs are enough to solve the FDI problem. We recall that our goal is not to condemn a given fault detection solution with respect to another one. Rather, the goal is to illustrate how the μ_g theory can be applied to any LTI FDI scheme.

5.3.2. Kalman estimator–based scheme

Let us now consider the design of a linear and stationary Kalman fault estimator. To proceed, the state equation (42) is considered with the assumption of parametric uncertainties and flexible modes, modelled as state disturbances $w(t)$. For the observation's equation (43), it is retained only the attitude angles $\Theta(t)$. For the fault model, we consider a signal $h(t)$ distributed through a matrix $\bar{H}$, so that $\bar{H}h(t) : h \in \mathbb{R}$ approximates the term $\sum_{i=1}^{4} H_i f_i(t)$ in (42). Typically, $\bar{H}$ is defined as the mean value of the absolute value of $H = [H_1 ... H_4]$ over the columns. With the dynamics of the fault model $\dot{h} = A_h h + w_h$, it can be verified that the fault detector design problem can be formulated as the design of a Kalman estimator for the following continuous-time plant (with the classical notations used in the Kalman theory):

$$\begin{cases} \dot{x}_e = \begin{bmatrix} A & \bar{H} \\ 0 & A_h \end{bmatrix} x_e + \begin{bmatrix} B \\ 0 \end{bmatrix} u + \begin{bmatrix} w(t) \\ w_h(t) \end{bmatrix} \\ y = \begin{bmatrix} C & 0 \end{bmatrix} x + v \end{cases} \quad \text{with } E\left\{ \begin{bmatrix} w(t) \\ w_h(t) \\ v(t) \end{bmatrix} \begin{bmatrix} w^T(\tau) & w_h^T(\tau) & v^T(\tau) \end{bmatrix} \right\} = \begin{bmatrix} Q & 0 \\ 0 & R \end{bmatrix} \delta(t-\tau) \tag{49}$$

In this equation, A, B, C refers to the state-space matrices of the model (42) under the modelling assumptions explained previously, and $\delta(t)$ refers to the Dirac impulse. Then, the last component

of the estimate $\hat{x}_e$ is nothing else than $\hat{h}$, the estimate of h, which provides the fault indicating signal r. The goal we pursue is to evaluate the performance of $r = \hat{h}$ against the uncertainties listed in table B.4, in the H_∞/H_- criteria sense.

To proceed, the fault estimator is inserted in the closed-loop model of the satellite, in a very similar manner than those illustrated on Fig. 10. Then, the model **N** is formed as illustrated on Fig.3.right, and μ_g, as-well-as the μ_g-sensitivities, are evaluated, see Fig.11 and 12. With regards to the objective functions W_d and W_f, the following result has been obtained:

$$\gamma_\Theta = 10,\ \gamma_\varpi = 10,\ \gamma_{f_1} \approx 0.1482,\ \gamma_{f_2} \approx 0.0445,\ \gamma_{f_3} \approx 0.0773,\ \gamma_{f_4} \approx 0.0356,\ \omega_f = 0.1rd/s$$

From the obtained results, it is interesting to note that:

- This solution has better fault sensitivity level than the pure H_∞/H_- fault detector and the UIO–based scheme, since parameters $\gamma_{f_i}, i = 1, ..., 4$ are bigger. The price to pay is, first, a less immunity against the measurement noise, especially against the star tracker noises since γ_Θ is a hundred times higher than for the case of the pure H_∞/H_- filter and ten times higher than for the case of the UIO scheme. Second, the magnitude of μ_g at the frequencies of the flexible modes, reveals a fault indicating signal very sensitive to the flexible mode effects compared to the pure H_∞/H_- solution, see Fig.11. This is confirmed by nonlinear simulations, see Fig.13.
- Compared to the case of the pure H_∞/H_- solution (see Fig. 8, the μ_g-sensitivities reveal that, for each faulty cases, the fault estimate $\hat{h}$ is particularly sensitive to uncertainties in the y and z components of the satellite's inertia matrix for frequencies lower than $0.01rd/s$.

Finally note that even if the performance of the Kalman estimator differ from the ones of the H_∞/H_- filter or the UIOs, they are enough to solve the fault detection problem, as it can be noted on Fig. 13. Again, our objective is not to condemn a given fault detection solution with respect to another one, but to demonstrate that the theories developed in this paper, provide useful tools to analyse the performance of any LTI fault detection scheme.

Remark 7. *It should be outlined that, even if we demonstrated that the μ_g theory can be applied successfully to a Kalman fault estimator, we cannot roughly speak about optimal performance in this particular case, since the μ_g theory is developed over H_∞/H_- criteria, whereas the Kalman solution is developed over a covariance criteria. The only conclusions we can draw are about the ability of the proposed Kalman scheme to be robust against uncertainties/disturbances in the H_∞-norm sense, and to be sensitive to the considered faults, in the H_- criteria sense.*

5.3.3. H_∞/H_- theory for performance enhancement

Let us come back to the UIO-based fault diagnosis solution addressed in section 5.3.1. In order to overcome the lack of performance of the UIO scheme, it is decided to post-filter the four UIOs by fusing all components of $e_i, i = 1, ..., 4$ by means of a H_∞/H_- filter. For that purpose, it suffices to define w_1 and w_2 as $w_1 = w_2 = e = [...e_i^T...]^T, i = 1, ..., 4 : e \in \mathbb{R}^{12}$. Then, by applying the theory presented in sections 3 and 4, we obtain a more robust and sensitive fault indicating signal r than those obtained my merging $e_i, i = 1, ..., 4$ through W, as it is revealed by Fig. 13.bottom. Details of this design are omitted here, but it is guaranteed that the synthesis technique follows the method presented in sections 3 and 4, with the characteristics for W_d and W_f that correspond to those fixed for the pure H_∞/H_- filter, see section 5.2.

6. Conclusion

The goal of the paper was to propose a set of tools for designing and analyse, robust H_∞/H_- fault detection and isolation solutions, for systems subject to many uncertainties, as well as disturbances. The design theory is approached using the non-smooth optimization techniques. A procedure that combines the benefit of the LMI-based optimization technique with the non-smooth theory, is discussed. A set of criteria for robust performance analysis within the H_∞/H_- framework, is proposed. The proposed measures are based on the generalized structured singular value μ_g. The proposed criteria enable to quantify the sensitivity of the residual vector against each uncertainties, to determine the combination of uncertainties that leads to fault detection performance loss and the frequency at which it occurs, and the combination of uncertainties that leads the performance margins to be the biggest, with the frequency at which it happens. A satellite's example is used to, first, illustrate how the presented theories can be applied, and second to demonstrate that the proposed theories are able to be applied to any LTI FDI scheme. An extension of the presented theories to the class of Linear Parameter Varying (LPV) systems, is under current research, thanks to the so-called L_2/L_--gains performance measures [20, 22] that generalize the H_∞/H_- criteria. The Integral Quadratic Constraint (IQC) formalism is expected to be a viable technique for that purpose.

Appendix A. PSO Algorithm

Algorithm 2 Pseudo code of the PSO algorithm

Initialize $p_s, c_1, c_2, \underline{\chi}, \overline{\chi}, q_\chi, q_L, \mathbf{x}_i, \mathbf{v}_i$, the maximum function evaluations $\overline{FE}$;
Set $\mathbf{p}_i^* = \mathbf{x}_i$ and find $\mathbf{g}^*$, set $FE = p_s$, the counter $k_L = 0$ and the iteration counter $k = 0$;
while $FE < \overline{FE}$ **do**
    By (31), update the inertia weight χ;
    for $k = 1$ to p_s **do**
        By (30), update the velocity and position of each particle;
        $FE = FE + 3$;
        if $f(\mathbf{x}_i) < f(\mathbf{p}_i^*)$ **then**
            $\mathbf{p}_i^* = \mathbf{x}_i$ and set $k_L = 0$;
        else
            $k_L = k_L + 1$;
        end if
        if $f(\mathbf{x}_i) < f(\mathbf{g}^*)$ **then**
            $\mathbf{g}^* = \mathbf{x}_i$;
        end if
    end for
    for $k = 1$ to p_s **do**
        if $k_L = q_L$ **then**
            By (32), generate a new position and replace $\mathbf{x}_i$;
            $FE = FE + 1$;
        end if
    end for
    $k = k + 1$;
end while

Appendix B. Characteristics of the satellite

	Symbols	Numerical values
Satellite's inertia	$J = diag(J_{xx}, J_{yy}, J_{zz})$	$J_{xx} = 14 \pm 10\% \quad kg.m^2$ $J_{yy} = 13 \pm 10\% \quad kg.m^2$ $J_{zz} = 19 \pm 10\% \quad kg.m^2$
Solar array's inertia	$J_{sa} = diag(J_{sa_{xx}}, J_{sa_{yy}}, J_{sa_{zz}})$	$J_{sa_{xx}} = 10 \pm 10\% \quad kg.m^2$ $J_{sa_{yy}} = 1 \pm 10\% \quad kg.m^2$ $J_{sa_{zz}} = 10 \pm 10\% \quad kg.m^2$
flexible mode's damping factors	$\xi = diag(\xi_1, \xi_2)$	$\xi_1 = \xi_2 = 3.10^{-3} \pm 20\%$
flexible mode's frequencies	$\omega_0 = diag(\omega_{0_1}, \omega_{0_2})$	$\omega_{0_1} = 1 \pm 20\% rd/s$ $\omega_{0_2} = 5 \pm 20\% \quad rd/s$
solar array modal participation matrix	B_R	$B_R = \begin{bmatrix} 36.6400 & 0 \\ 0 & 0.0600 \\ 0 & -37.0100 \end{bmatrix}$

Table B.4: Characteristics of the satellite

References

[1] Apkarian, P., 2011. Nonsmooth μ-synthesis. International Journal of Robust and Nonlinear Control 21 (13), 1493–1508.

[2] Apkarian, P., Doll, N., 2006. Nonsmooth H_∞ synthesis. IEEE Transaction on Automatic Control 51 (1), 71–86.

[3] Apkarian, P., Noll, D., Rondepierre, A., 2008. Mixed H_2/H_∞ control via nonsmooth optimization. SIAM Journal on Control and Optimization 47 (3), 1516–1546.

[4] Basseville, M., Nikiforov, I., 1993. Detection of abrupt changes. Theory and application. Prentice hall information and system sciences series.

[5] Bertsekas, D., 1995. Nonlinear programming. Athena Scientific, USA, Belmont, Mass.

[6] Bruinsma, N., Steinbuch, M., 1990. A fast algorithm to compute the H_∞-norm of a transfer function matrix. System and Control Letters 14 (5), 287–293.

[7] Clarke, F., 1983. Optimization and Nonsmooth Analysis. Canadian Math. Soc. Series. John Wiley & Sons, New York.

[8] Cockburn, J., Morton, B., 1997. Linear fractional representations of uncertain systems. Automatica 33 (7), 1263–1271.

[9] Colmenarejo, P., Branco, J., Santos, N., Arroz, P., Telaar, J., Strauch, H., Ott, C., Reiner, M., Henry, D., Jaworski, J., Papadopoulos, E., Visentin, G., Ankersen, F., Gil-Fernandez, J., 2018. Methods and outcomes of the comrade project - design of robust coupled control for robotic spacecraft in servicing missions: trade-off between H_∞ and nonlinear lyapunov-based approaches. In: International Astronautical Congress. Bremen. Germany.

[10] Da Silva de Aguiar, R., Apkarian, P., Noll, D., 2018. Structured robust control against mixed uncertainty. IEEE Transactions on Control Systems Technology 26 (5), 1771–1781.

[11] Ding, S., Jeinsch, T., Frank, P., Ding, E., 2000. A unified approach to the optimization of fault detection systems. International Journal of Adaptive Control and Signal Processing 14, 725–745.

[12] Ding, S. X., April 10 2008. Model–based Fault Diagnosis Techniques: Design Schemes, Algorithms, and Tools, 1st Edition. Springer, Berlin Heidelberg, ISBN: 978–3540763031.

[13] Fan, M., Tits, A., Doyle, J., 1991. Robustness in the presence of mixed parametric uncertainty and unmodeled dynamics. IEEE Transactions on Automatic Control 36 (1), 25–38.

[14] Fonod, R., Henry, D., Charbonnel, C., Bornschlegl, E., 2015. Position and attitude model-based thruster fault diagnosis: A comparison study. AIAA Journal of Guidance, Control, and Dynamics 38 (6), 1012–1026.

[15] Fonod, R., Henry, D., Charbonnel, C., Bornschlegl, E., Losa, D., Bennani, S., 2015. Robust FDI for fault-tolerant thrust allocation with application to spacecraft rendezvous. Control Engineering Practice 42, 12–27.

[16] Gahinet, P., Apkarian, P., 1994. A linear matrix inequality approach to H_∞ control. Int. Journal Robust Nonlinear Control 4, 421–428.

[17] Gao, N., Darouach, M., Voos, H., Alma, M., 2016. New unified H_∞ dynamic observer design for inear systems with unknown inputs. Automatica 65, 43–52.

[18] Hecker, S., Varga, A., Magni., J., 2005. Enhanced LFR-toolbox for matlab. Aerospace Science and Technology 9, 173–180.

[19] Henry, D., 2008. Fault diagnosis of the Microscope satellite actuators using H_∞/H_- filters. AIAA Journal of Guidance, Control, and Dynamics 31 (3), 699–711.

[20] Henry, D., 2012. Structured fault detection filters for LPV systems modeled in a LFR manner. International Journal of Adaptive Control and Signal Processing 26 (3), 190–207.

[21] Henry, D., Cieslak, J., Zolghadri, A., Efimov, D., 2014. A non-conservative H_-/H_∞ solution for early and robust fault diagnosis in aircraft control surface servo-loops. Control Engineering Practice 31, 183–199.

[22] Henry, D., Cieslak, J., Zolghadri, A., Efimov, D., 2015. H_∞/H_- LPV solutions for fault detection of aircraft actuator faults: Bridging the gap between theory and practice. International Journal of Robust and Nonlinear Control 25 (5), start page 649.

[23] Henry, D., LePeuvédic, C., Strippoli, L., Ankersen, F., 2015. Robust model-based fault diagnosis of thruster faults in spacecraft. In: SAFEPROCESS'2015. Ifac, Paris, France, pp. 1078–1083.

[24] Henry, D., Zolghadri, A., 2005. Design and analysis of robust residual generators for systems under feedback control. Automatica 41, 251–264.

[25] Henry, D., Zolghadri, A., 2005. Design of fault diagnosis filters: A multi-objective approach. Journal of Franklin Institute 342 (4), 421–446.

[26] Henry, D., Zolghadri, A., 2006. Norm-based design of robust fdi schemes for uncertain systems under feedback control: Comparison of two approaches. Control Engineering Practice 14 (9), 1081–1097.

[27] Iwasaki, T., Hara, S., 2005. Generalized kyp lemma: unified frequency domain inequalities with design applications. IEEE Transactions on Automatic Control 50 (1), 41–59.

[28] Kennedy, J., Eberhart, R., 1995. Particle swarm optimization. In: Proceedings of ICNN'95 - International Conference on Neural Networks. Vol. 4. pp. 1942–1948 vol.4.

[29] Khosrowjerdi, M., Nikoukhah, R., Safari-Shad, N., 2004. A mixed H_2/H_∞ approach to simultaneous fault detection and control. Automatica 40 (2), 261–267.

[30] Lungu, M., Lungu, R., 2014. Design of full-order observers for systems with unknown inputs by using the eigenstructure assignment. Asian J. Control 16 (5), 1470–1481.

[31] Marcos, A., 2012. Assessment on the addsafe benchmark simulator of an H_∞ fault detection design for aircraft. In: 8th IFAC SAFEPROCESS. Mexico.

[32] Mezura-Montes, E., Coello], C. A. C., 2011. Constraint-handling in nature-inspired numerical optimization: Past, present and future. Swarm and Evolutionary Computation 1 (4), 173 – 194.

[33] Morris, J., Newlin, M., 1995. Model validation in the frequency domain. In: Proceedings of the 34th Conference on Decision and Control. New Orleans - USA, pp. 3582–3587.

[34] Palhares, R., Peres, P., 2000. Robust H_∞ filter design with pole constraints for discrete-time systems. Journal of the Franklin Institute 337, 713–723.

[35] Pedersen, M. E. H., 2010. Good Parameters for Particle Swarm Optimization.

[36] Peter, O., 2014. Introduction to Partial Differential Equations. Chapter 5. Vol. 10.1007/97. Springer.

[37] Pittet, C., Falcoz, A., Henry, D., 2016. A model-based diagnosis method for transient and multiple faults of aocs thrusters. In: 20th IFAC Symposium on Automatic Control in Aerospace ACA 2016. Vol. 49. IFAC, Sherbrooke, Quebec, Canada, pp. 82–87.

[38] Reppa, V., Polycarpou, M. M., Panayiotou, C. G., 2015. Decentralized isolation of multiple sensor faults in large-scale interconnected nonlinear systems. IEEE Transactions on Automatic Control 60 (6), 1582–1596.

[39] Saberi, A., Stoorvogel, A., Sannuti, P., Niemann, H., 2000. Fundamental problems in fault detection and identification. International Journal of Robust and Nonlinear Control 10 (14), 1209–1236.

[40] Sharma, V., Sharma, B.-B., Nath, R., 2018. Unknown input reduced order observer based synchronization framework for class of nonlinear systems. Int. J. Dynam. Control 6, 1111–1125.

[41] Stoorvogel, A., Niemann, H., Saberi, A., Sannuti, P., 2002. Optimal fault signal estimation. International Journal of Robust and Nonlinear Control 12 (8), 697–727.

[42] Stoustrup, J., Niemann, H., 2002. Fault estimation-a standard problem approach. International Journal of Robust and Nonlinear Control 12 (8), 649–673.

[43] Wang, C., Liu, K., 2018. An improved particle swarm optimization algorithm based on comparative judgment. Natural Computing 17, 641–661.

[44] Wang, H., Yang, G., 2007. Fault detection observer design in low frequency domain. In: 2007 IEEE International Conference on Control Applications. pp. 976–981.

[45] Wang, H., Yang, G.-H., 2008. A finite frequency domain approach to fault detection for linear discrete-time systems. International Journal of Control 81 (7), 1162–1171.

[46] Wang, J., Yang, G.-H., Liu, J., 2007. An LMI approach to H_- index and mixed H_-/H_∞ fault detection observer design. Automatica 43 (9), 1656–1665.

[47] Wei, X., Verhaegen, M., 2010. Robust fault detection observer and fault estimation filter design for lti systems based on gkyp lemma. European Journal of Control 16 (4), 366–383.

[48] Xue, T., Zhong, M., Ding, S. X., Ye, H., 2018. Stationary wavelet transform aided design of parity space vectors for fault detection in ldtv systems. IET Control Theory Applications 12 (7), 857–864.

[49] Young, P. M., Doyle, J. C., 1997. A lower bound for the mixed μ problem. IEEE Transactions on Automatic Control 42 (1), 123–128.

[50] Zhong, M., Song, Y., Ding, S., 2015. Parity space-based fault detection for linear discrete time-varying systems with unknown input. Automatica 59, 120–126.

[51] Zhou, K., Doyle, J., Glover, K., 1996. Robust and Optimal Control. Prentice Hall.

[52] Zhou, M., Wang, Z., Shen, Y., 2017. Fault detection and isolation method based on H_-/H_∞ unknown input observer design in finite frequency domain. Asian Journal of Control 19 (5), 1777–1790.

[53] Zolghadri, A., Henry, D., Cieslak, J., Efimov, D., Goupil, P., 2014. Fault Diagnosis and Fault-Tolerant Control and Guidance for Aerospace Vehicles: From theory to application. Springer, Series: Advances in Industrial Control. ISBN 978-1-4471-5312-2.

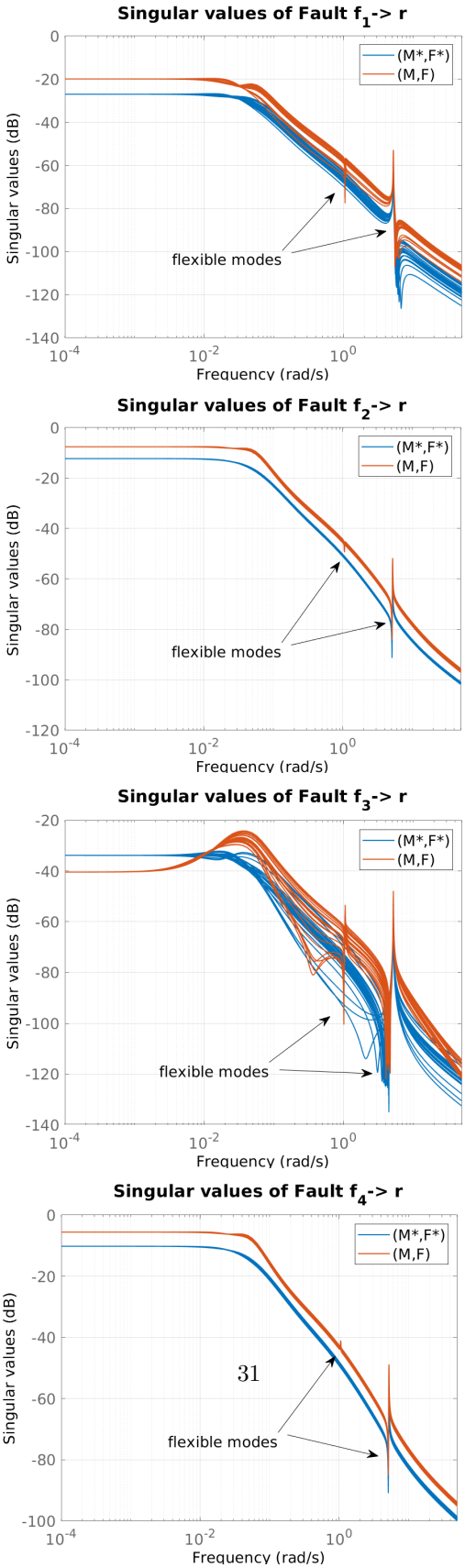

Figure 6: Sigma plots of $T_{f_i r}(j\omega), i = 1, ..., 4$ (from top left to bottom right)

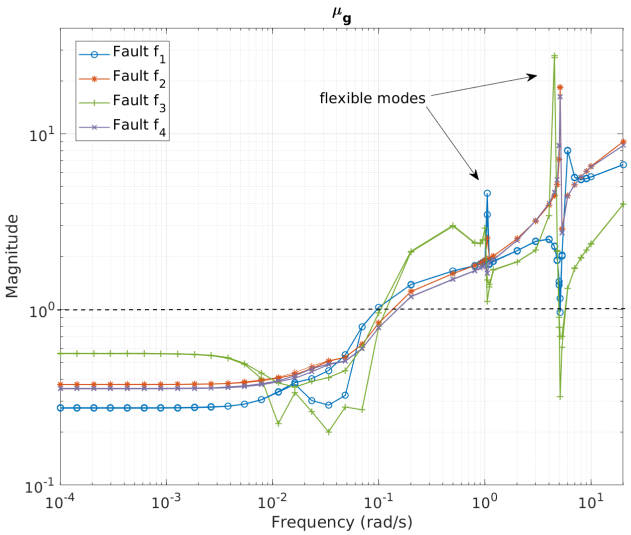

Figure 7: The μ_g function $\mu_{g\underline{\mathbf{\Delta}}}\left(\mathbf{N}(s)\right), s = j\omega$

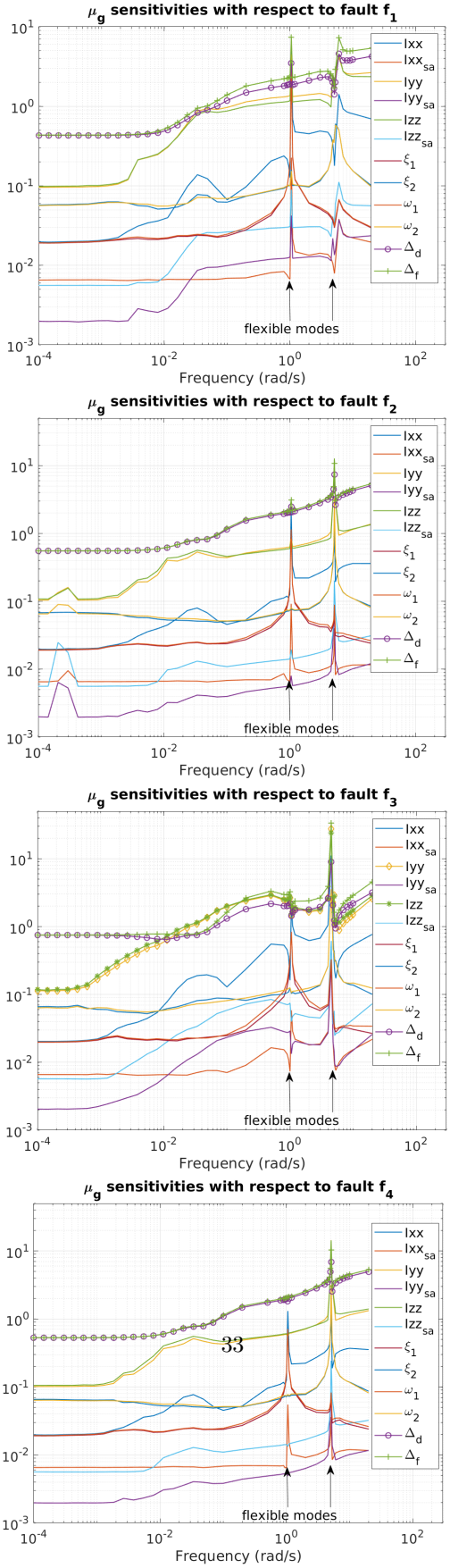

Figure 8: The μ_a-sensitivities $\mathcal{S}\mu_a^i(\omega)$ for fault $i = 1, ..., 4$ (from top left to bottom right)

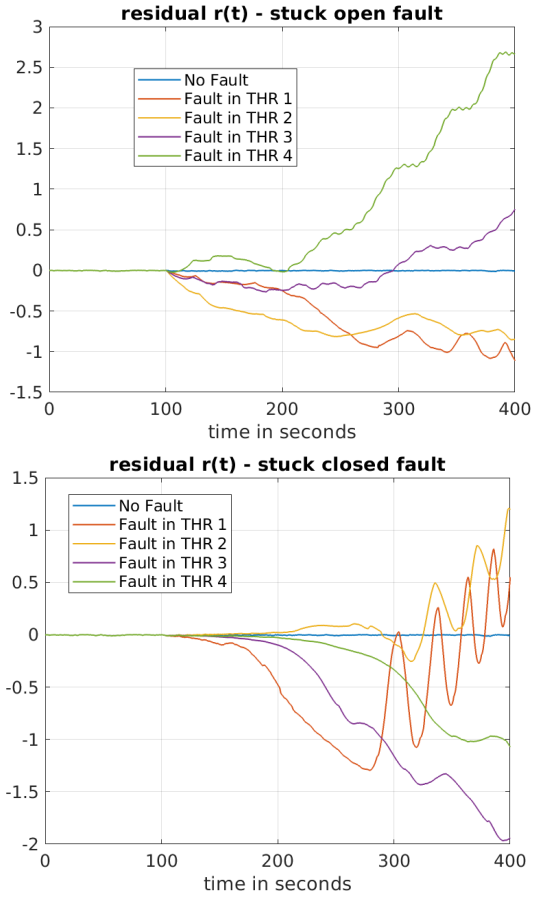

Figure 9: $r(t)$ for stuck-open faults (left) and stuck-closed faults (right)

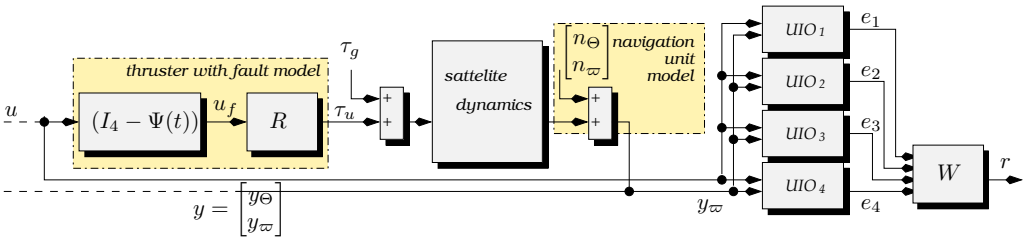

Figure 10: The UIO-based FDI unit

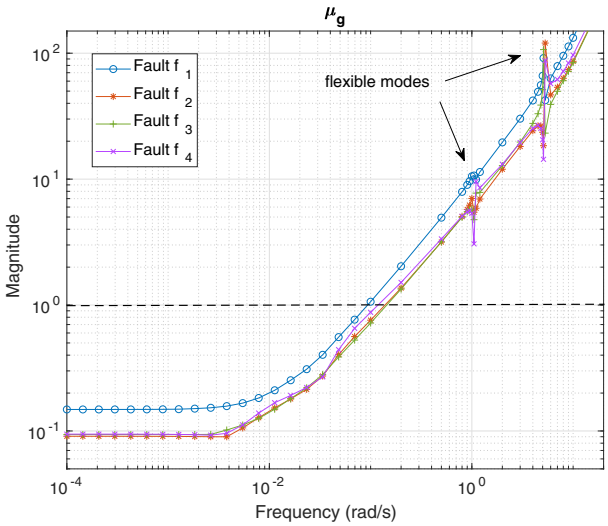

Figure 11: The μ_g function $\mu_{g\underline{\Delta}}\left(\mathbf{N}(s)\right), s = j\omega$ - Kalman fault estimator

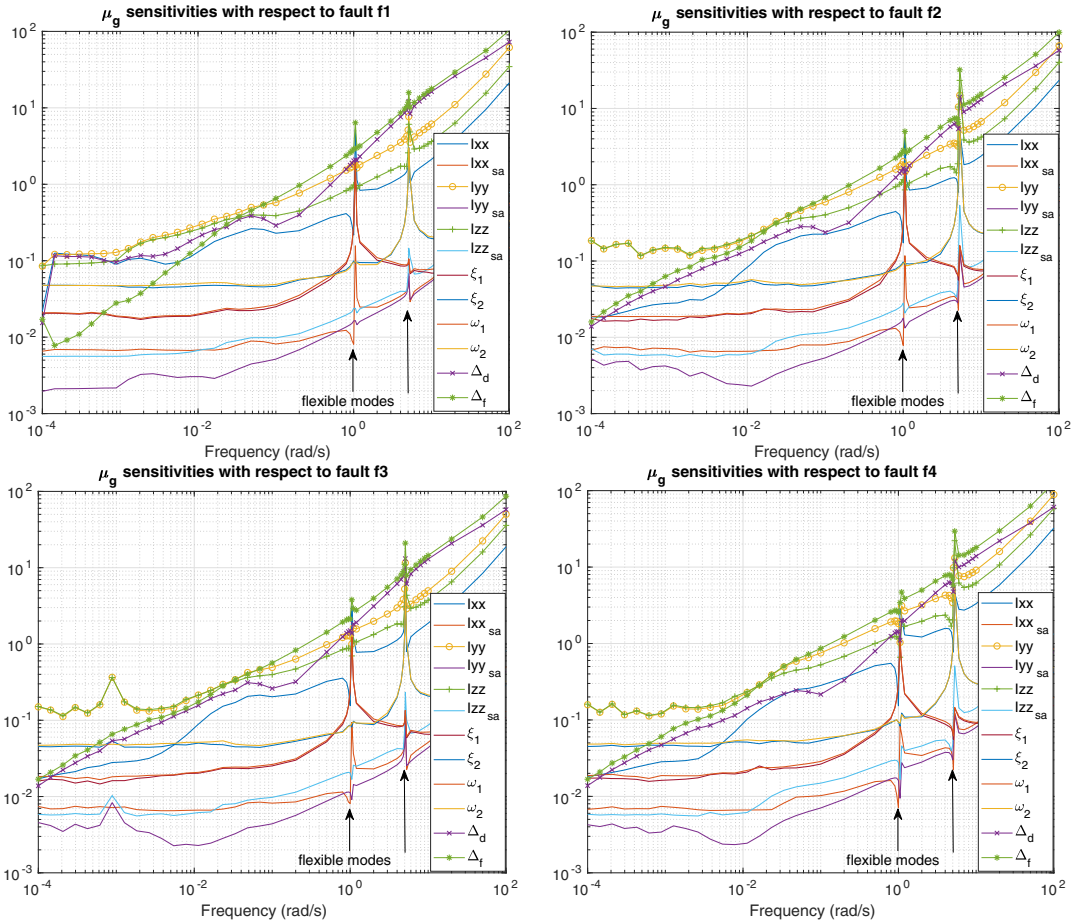

Figure 12: The μ_g-sensitivities $\mathcal{S}\mu_g^i(\omega)$ for fault $i = 1, ..., 4$ (from top left to bottom right) - Kalman fault estimator

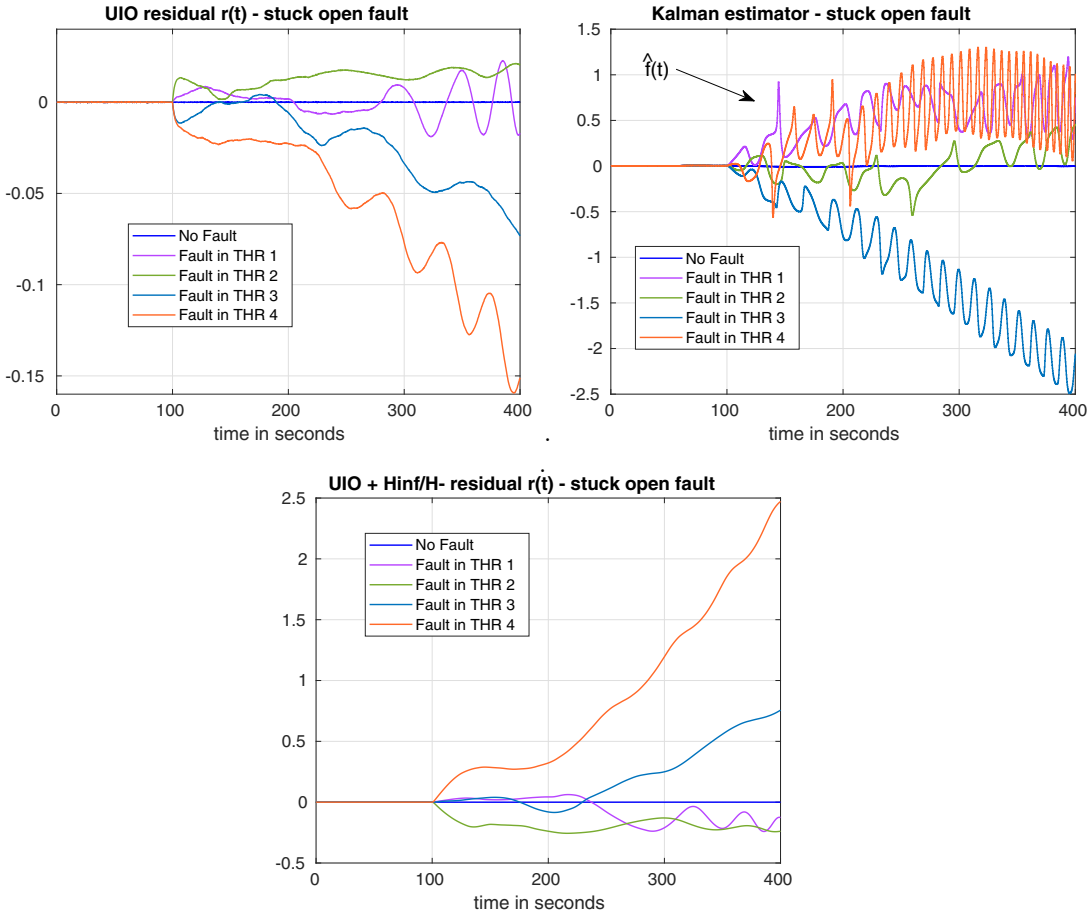

Figure 13: Behaviour of the fault indicating signal for stuck-open faults. Pure UIO (top left), Kalman–based estimate (top right) and UIO with H_∞/H_- post-filtering (bottom)